

## VOLTAGE-CLAMP FREQUENCY DOMAIN ANALYSIS OF NMDA-ACTIVATED NEURONS

L. E. MOORE\*

*Department of Physiology and Biophysics, University of Texas Medical Branch,  
Galveston, Texas 77550, USA and Equipe de Neurobiologie, Neuropharmacologie  
Moléculaire et Ecotoxicologie, C.N.R.S., Université de Rennes I, 35042 Rennes Cedex,  
France*

R. H. HILL and S. GRILLNER

*The Nobel Institute for Neurophysiology, Karolinska Institute, Stockholm, Sweden*

*Accepted 23 September 1992*

### Summary

1. Voltage and current-clamp steps were added to a sum of sine waves to measure the tetrodotoxin-insensitive membrane properties of neurons in the intact lamprey spinal cord. A systems analysis in the frequency domain was carried out on two types of cells that have very different morphologies in order to investigate the structural dependence of their electrophysiological properties. The method explicitly takes into account the geometrical shapes of (i) nearly spherical dorsal cells with one or two processes and (ii) motoneurons and interneurons that have branched dendritic structures. Impedance functions were analysed to obtain the cable properties of these *in situ* neurons. These measurements show that branched neurons are not isopotential and, therefore, a conventional voltage-clamp analysis is not valid.

2. The electrophysiological data from branched neurons were curve-fitted with a lumped soma-equivalent cylinder model consisting of eight equal compartments coupled to an isopotential cell body to obtain membrane parameters for both passive and active properties. The analysis provides a quantitative description of both the passive electrical properties imposed by the geometrical structure of neurons and the voltage-dependent ionic conductances determined by ion channel kinetics. The model fitting of dorsal cells was dominated by a one-compartment resistance and capacitance in parallel (RC) corresponding to the spherical, non-branched shape of these cells. Branched neurons required a model that contained both an RC compartment and a cable that reflected the structure of the cells. At rest, the electrotonic length of the cable was about two. Uniformly distributed voltage-dependent ionic conductance sites were adequate to describe the data at different membrane potentials.

3. The frequency domain admittance method in conjunction with a step voltage clamp was used to control and measure the oscillatory behavior induced by *N*-methyl-D-aspartate (NMDA) on lamprey spinal cord neurons. Voltage-clamp currents and

\*Present address: Equipe de Neurobiologie, Neuropharmacologie Moléculaire et Ecotoxicologie, C.N.R.S., Université de Rennes I, 35042 Rennes Cedex, France.

impedance functions were measured at different membrane potentials. The impedance functions had a voltage-dependent resonance and phase shift characteristic of a negative conductance. These measurements provide a quantitative analysis of the conductances induced by NMDA in central neurons of the lamprey spinal cord and directly establish the basis of the non-linear oscillatory behavior previously observed in the presence of NMDA. NMDA was shown specifically to activate a negative and a positive conductance, both of which were markedly affected by the membrane potential. It is shown that the net current in the presence of NMDA must be considered as the algebraic sum of currents in opposite directions.

4. The impedance functions at membrane potentials hyperpolarized by  $-10\text{mV}$  or more were described by passive properties. However, at less negative potentials the neurons showed a non-resonating enhancement of the impedance magnitude with a clear negative conductance revealed by a phase function more negative than  $-90^\circ$ . For modest depolarizations of less than  $10\text{mV}$ , a sharp resonance and phase function were observed. Finally, at greater depolarizations, a broader resonance with a less abrupt phase change occurred. In the potential range of NMDA-induced oscillatory behavior, the observed impedance resonance peaks were in the range of the oscillation frequencies of neurons seen under current-clamp conditions.

5. The NMDA-induced negative conductance was reduced by the removal of  $\text{Na}^+$  without blocking an NMDA-enhanced positive conductance, which is consistent with the hypothesis that NMDA directly induces a voltage-dependent conductance to both  $\text{Ca}^{2+}$  and  $\text{Na}^+$ . The NMDA-induced positive conductance remaining after  $\text{Na}^+$  removal is probably a consequence of the activation of a potassium conductance by increased intracellular calcium levels. The frequency of the NMDA-induced resonance was decreased by the removal of  $\text{Na}^+$ . In the presence of  $\text{Na}^+$  and NMDA, the resonance is a mixture of outward and inward current kinetics, the combination of which leads to a lower peak frequency the greater the inward current.

6. These experiments show that activation of the NMDA receptor leads to an inherently unstable condition where a negative conductance depolarizes the cell. This then turns on a repolarizing positive conductance. The activation of both the NMDA-induced inward current and a positive conductance contributes to a resonance in the impedance that will influence the inherent oscillation frequency. Finally, the voltage-dependent impedance markedly affects the cable properties of the neurons and their ability to propagate synaptic potentials.

## Introduction

Electrophysiological measurements of the properties of neurons within an intact nervous system have been severely limited because classical voltage-clamp methodology cannot be applied to cells with dendritic processes. The cable properties of such neurons have been investigated using experimental and theoretical approaches pioneered by Rall (Rall, 1959, 1969). These analyses have usually not considered that the voltage-dependent ion channels may be gated even at membrane potentials near the resting level. One way to evaluate such a complex system is with systems analysis methods (Marmarelis and Marmarelis, 1978) to obtain transfer functions that allow an analysis of synaptic integrative processes. At the single cell level, linear transfer functions have often

been obtained in the frequency domain to allow measurement of responses which encompass all frequencies of biological interest (Fishman *et al.* 1977) and provide data to construct realistic models with cable structures (Moore and Tsai, 1983). Generally, measurements made on neurons are from a single point, the soma, and thus are referred to as driving point functions since the stimulus and response occur at the same location.

A frequency domain analysis has been developed for estimating cable properties in cultured neurons (Moore and Christensen, 1985; Moore *et al.* 1988; Yoshii *et al.* 1988). In these studies good agreement was found between measured driving point functions and those estimated from models based on cell geometry. The experiments reported here are a direct extension of the techniques developed in cultured cells to neurons in an intact spinal cord of the lamprey in order directly to measure driving point functions to obtain models that can determine the shape of synaptic potentials. The lamprey brain stem and spinal cord (Rovainen, 1974, 1978, 1979) preparation was chosen because of its extensive use as a lower vertebrate model for central nervous functions (Grillner *et al.* 1987*b*). In order to evaluate the contribution of voltage-sensitive membrane parameters to cellular electrical properties it is important to obtain driving point functions of lamprey neurons at different membrane potentials (Moore *et al.* 1986, 1987*a,b*). A specific purpose of the experiments presented here was to develop a method to measure the membrane properties of intact neurons of the spinal cord, including those that are induced by neurotransmitters.

Non-linear electrical properties, such as those found in neurons, can be described with linear analysis by doing piece-wise linearization. In an excitable cell this is achieved by small signal perturbations about different mean membrane potentials (Moore *et al.* 1980). Thus, linear analysis provides a description not only of passive circuit elements but also of voltage-gated ion channel properties at different levels of membrane potential. Although a structure like a neuron with dendrites will probably not be uniformly space voltage-clamped, it is possible to displace the potential of the soma by a few millivolts and measure responses due to voltage-dependent conductances from the entire cell (Hodgkin and Huxley, 1952; Mauro *et al.* 1970). The driving point function analysis provides kinetic data for models (Moore and Buchanan, 1993) of branched structures over a limited range of membrane potentials that otherwise cannot be easily obtained.

Neurotransmitters are known to gate ion channels in addition to the normal voltage-dependent conductances. Among these are the excitatory amino acids with multiple subtypes, namely, *N*-methyl-D-aspartate (NMDA) and non-NMDA receptors (Ascher and Nowak, 1988; MacDonald *et al.* 1982; Watkins, 1981; Watkins *et al.* 1986). Certain unitary ESPSs that are dependent on NMDA receptor activation (Buchanan *et al.* 1987; Bekkers and Stevens, 1989; Dale and Grillner, 1986) can be distinguished both by a voltage dependency and by an ability to open channels for calcium ions as well as for other cations (MacDermott *et al.* 1986). At a larger system level, the activation of NMDA receptors can lead to membrane potential oscillations, which play an important role in rhythmic behavior (Brodin and Grillner, 1986; Dale and Roberts, 1984, 1985; Dale and Grillner, 1986; Grillner *et al.* 1981; Wallén and Grillner, 1987; Sigvardt *et al.* 1985).

Most quantitative investigations of NMDA actions have been carried out on isolated cultured cells or hippocampal slice preparations (Ascher and Nowak, 1988; Cull-Candy and Usowicz, 1987, 1989*a,b*; Dingledine, 1986; Flatman *et al.* 1986; Jahr and Stevens,

1987; Llano *et al.* 1988; Mayer and Westbrook, 1985, 1987*a,b*; Nowak *et al.* 1984). The present series of experiments was performed on the isolated lamprey spinal cord (*Ichthyomyzon unicuspis*) in which bath application of NMDA evokes an organized motor activity analogous to normal locomotion (Grillner *et al.* 1981, 1982, 1987*a*; Brodin *et al.* 1985; Buchanan and Cohen, 1982; Wallén and Williams, 1984). Synaptic events elicited during NMDA-induced fictive locomotion exhibit a voltage dependence (Moore *et al.* 1987*a*) consistent with an endogenous activation of NMDA receptors (Brodin and Grillner, 1985; Buchanan and Grillner, 1987; Dale, 1986; Moore *et al.* 1987*a,b*). Although bath-applied NMDA may activate extrasynaptic receptors, this procedure is useful for the evaluation of the membrane properties induced by NMDA that are likely to be occurring at postsynaptic sites during locomotion. The most dramatic effect of such NMDA bath application is the induction of endogenous membrane potential oscillations after action potentials have been abolished by tetrodotoxin (TTX) (Sigvardt *et al.* 1985). These TTX-insensitive, 2–20mV oscillations are dependent on sodium, calcium and magnesium ions, where the latter confer a voltage dependence on the site (Grillner and Wallén, 1985; Wallén and Grillner, 1987). This oscillatory activity (Llinàs, 1988) is due to a negative conductance brought about by a voltage-dependent magnesium block (Ault *et al.* 1980; Nowak *et al.* 1984) of the NMDA-activated channel that acts in combination with other channels.

The experiments reported here investigate the membrane properties induced by NMDA receptor activation of intact neurons in order to assess the role they may play in integration of synaptic potentials in the locomotor neural circuit. Using frequency domain methods, a kinetic analysis of the passive and active membrane properties of intact motor neurons and interneurons of the lamprey spinal cord during NMDA receptor activation has been carried out. Potential-dependent impedance functions (Moore and Christensen, 1985) were obtained in an analysis that explicitly takes into account both the active and passive membrane properties of cable structures and provides an assessment of the integrative properties of individual central neurons. In the presence of NMDA, the impedance had a resonance and phase behavior characteristic of a negative conductance. These measurements provide a quantitative analysis of the conductances induced by NMDA in central neurons and directly establish the basis of the non-linear oscillatory behavior previously observed in the presence of NMDA (Grillner and Wallén, 1985; Wallén and Grillner, 1987).

### Materials and methods

The lamprey spinal cord was isolated with or without the notochord and mounted in a perfused temperature-controlled chamber at 8–10°C. Suction electrodes were used to record ventral root activity for the identification of motoneurons. One hundred and twelve neurons were investigated out of which fourteen were identified as motoneurons. Most cells could not be identified because they were bathed in TTX to block sodium channels and reduce synaptic noise. Fig. 1 illustrates the recording arrangement and the driving point function measurements under voltage-clamp conditions. The stimulus consists of a step voltage command where the duration has been extended in order to add a

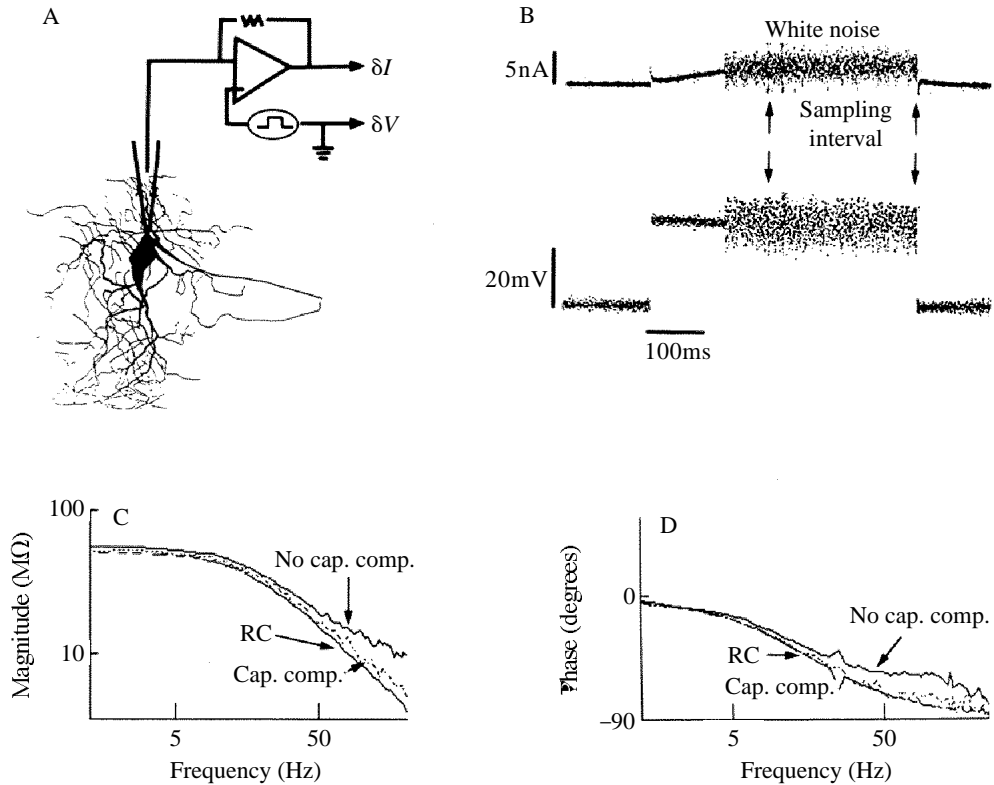


Fig. 1. The combination voltage-clamp and sum of sines method. (A) The single-electrode voltage-clamp is diagrammatically indicated. The electrode is shown in the soma of the reconstructed neuron. A planar superposition of 12 optical planes of a Lucifer-filled motor neuron that was reconstructed using measurements from photographic prints shows the principal dendrites and branches. The command voltage,  $\delta V$ , leads to a current,  $\delta I$ . (B) The voltage-clamp responses for the activation of an outward current show how the sum of sines signals are summed with the step voltage-clamp after the transient response has settled. Note that the data for the FFT analysis are collected after a delay to allow for a steady-state response. The magnitude and phase functions of C and D show the effect of electrode negative capacitance compensation on the measurement of a known RC parallel network. Magnitude and phase functions are shown for three superimposed traces representing (1) a parallel resistance and capacitance, RC (50 M $\Omega$  and 200 pF), directly measured, (2) the impedance of the same RC but measured through a 70 M $\Omega$  electrode to ground with insufficient negative capacitance compensation (no cap. comp.), and (3) impedance of the RC circuit with the electrode and nearly adequate negative capacitance compensation (cap. comp.). The impedance measured with adequate compensation superimposes on that of 1.

superimposed white noise stimulus. A fast Fourier transform (FFT) was used to compute the driving point function either as an admittance,  $Y$ , or its reciprocal, an impedance,  $Z$ , as a function of frequency. The details of the driving point function method have been published previously (Poussart *et al.* 1977; Moore and Tsai, 1983; Moore and Christensen, 1985; Fox and Chan, 1985). Essentially a conventional voltage- or current-clamp step pulse is summed with a group of sine waves that have constant amplitudes and

randomized phases. The root mean square (r.m.s) amplitude of the sine waves was comparatively small ( $<3\text{mV}$ ) in order to elicit a linear response from the cell. The composite of sine waves was summed to the step change after the main part of the transient response had settled in order to achieve a steady state and to allow the measurement of the more conventional large signal relaxations during the same pulse as the driving point function. The measurements were made during a voltage or current clamp from a single electrode and are referred to as point impedance ( $\delta V/\delta I$ ) or driving point functions. The driving point function was measured under voltage-clamp conditions for different neurons and included identified motor neurons. The responses are presented as relative sine wave amplitudes (magnitudes) and their corresponding phase shifts compared to the phase of the stimulating sine wave. Although the phases have been randomized to generate the white noise, they are absolutely identical for each measurement. Therefore, a single reference can be used for multiple measurements. Thus, each sine wave response is represented by two points, the magnitude and the phase, both of which are then plotted as a function of frequency. All of the driving point functions are plotted as point impedances, but the measurements were usually carried out under-voltage-clamp conditions. In addition to the magnitude,  $Z$ , and phase,  $\theta$ , the data were expressed as a complex impedance using the standard expressions for conversion between these two forms, namely,  $Z^2=R_e^2+J_m^2$  and  $\tan\theta=J_m/R_e$ , where  $R_e$  is the real and  $J_m$  the imaginary, part of the impedance. These data were plotted as  $J_m$  versus  $R_e$ , known as an impedance plane plot.

Generally, voltage-clamp admittance measurements,  $Y(f)=\delta I(f)/\delta V(f)$ , were made, where, at a single point in the neuronal soma, the current ( $\delta I$ ) was measured in response to a controlled, white noise modulated, reference voltage ( $\delta V$ ) command. In control experiments, constant current impedances,  $Z(f)=\delta V(f)/\delta I(f)$ , were measured and shown to be identical to the reciprocal of the admittance functions. Although voltage-clamp studies have the advantage of controlling the non-linearity of the system, they suffer from the disadvantage that the voltage control as a function of frequency is dependent on the gain, the phase shift and the capacitance neutralization used in the feedback system. A determination of one part of the linear response was made by the observation of symmetry in current response to opposite changes in the membrane potential (see Fig. 4Biii). In addition, driving point function measurements for different peak-to-peak white noise stimuli showed a linear response for white noise measurements with r.m.s. voltage values of  $\pm 2\text{--}5\text{mV}$  (Moore *et al.* 1980).

All measurements were made with a switching current or voltage clamp (Axoclamp-2, Axon Instruments, Burlingame, California) using both thin- and thick-walled glass microelectrodes filled with  $4\text{mol l}^{-1}$  potassium acetate whose d.c. resistances were  $25\text{--}70\text{M}\Omega$ . It was necessary to monitor the voltage at the input of the sample-and-hold amplifier used in the discontinuous clamp to ensure that its decay after the current injection part of the duty cycle was complete. Capacitance compensation was monitored and adjusted to remove the electrode transients during the recording phase of the duty cycle. The switching frequency used was  $1.5\text{--}2\text{kHz}$  for the  $200\text{Hz}$  measurement band and  $2\text{--}5\text{kHz}$  for the  $500\text{Hz}$  band. It was generally not possible to obtain adequate capacitance compensation using electrodes with resistances above  $80\text{M}\Omega$ . Furthermore,

the fluid level and the impedance characteristics of individual spinal cords were factors that affected the compensation.

In addition to the single-electrode measurements, control two-electrode model experiments showed identical impedance functions if each electrode was adequately shielded. Control measurements from a model RC circuit (see legend of Fig. 1) grounded through a 70M $\Omega$  microelectrode showed that 25–70M $\Omega$  electrodes can be used in the range 0–500Hz. Fig. 1C,D illustrates the critical nature of the capacitance neutralization required with the switching clamp. The superimposed impedance functions illustrate the distortion of phase function when the capacitance compensation is insufficient (Fig. 1D).

The voltage-clamp steps encompassed the range of membrane potentials observed in oscillating spinal neurons during fictive locomotion. All experiments were carried out at 8–11°C in the presence of 3  $\mu\text{mol l}^{-1}$  TTX to prevent synaptic noise and uncontrolled action potentials. The normal lamprey Ringer's solution had the following composition (in  $\text{mmol l}^{-1}$ ): 115 NaCl, 2.1 KCl, 2.6 CaCl<sub>2</sub>, 2.0 MgCl<sub>2</sub>, 3 NaHCO<sub>3</sub> and 3 glucose. Since NMDA depolarized the neurons, cells in NMDA solutions were held by the voltage clamp at –50mV, unless otherwise stated in the figure legends.

The data reported were selected from impedance measurements on 112 neurons, 14 of which were identified motoneurons. The effects of NMDA were investigated on 45 unidentified neurons and 8 identified motoneurons. NMDA (100  $\mu\text{mol l}^{-1}$ ) was applied in the perfusion bath and its effects were investigated only on neurons that showed spontaneous potential oscillations. The effects of the removal of sodium ions were studied in six neurons. It is assumed that many of the unidentified neurons were motoneurons since these are numerous and easy to impale with the low-resistance electrodes (<50 M $\Omega$ ) filled with 4mol<sup>-1</sup> potassium acetate that were typically used in these experiments.

### Theoretical basis

As discussed above, the impedance function contains far more information about a neuron than its passive properties. Although it has been shown (Mauro *et al.* 1970; Fishman *et al.* 1977; Koch, 1984) that the small signal linear impedance is a measurement of the voltage-dependent conductances as well as the passive cable properties of an excitable cell, a brief derivation of the admittance function for a single ion under voltage-clamp conditions will be given. Using the Hodgkin–Huxley formula (Hodgkin and Huxley, 1952) as follows:

$$I = g_{\max} n^x (V - V_e) + C(dV/dt), \quad (1)$$

where the current is  $I$ ,  $g_{\max}$  is the maximum chord conductance,  $n$  is a voltage-dependent variable having values between 0 and 1,  $x$  is an exponent usually having a value of 2–4,  $V$  is the membrane potential,  $V_e$  is the reversal potential for the current,  $t$  is time, and  $C$  is the membrane capacitance. The voltage-dependent kinetics are given by Hodgkin and Huxley (1952):

$$dn/dt = \alpha(1 - n) - \beta(n), \quad (2)$$

where  $\alpha$  and  $\beta$  are forward and reverse rate constants for closed and open conducting states. Small signal perturbations (Mauro *et al.* 1970) give:

$$\delta I = C d(\delta V)/dt + g_{\max}(n - x)\delta V + xn^{(x-1)}g_{\max}(V - V_e)\delta n, \quad (3)$$

where  $n = \alpha/(\alpha + \beta)$  is the steady-state value of  $n$  at a specified voltage. Taking the differential  $[d(\delta n)/dt]$  of  $dn/dt$  (Mauro *et al.* 1970) and defining  $\alpha_V = d\alpha/dV$  and  $\beta_V = d\beta/dV$ , the membrane admittance ( $Y$ ) is given by:

$$Y = \delta I/\delta V = j\omega C + g_{\max}n^x + x[n^{(x-1)}]g_{\max}(V - V_e)\tau\{\alpha_V - n(\alpha_V + \beta_V)\}/(1 + j\omega\tau), \quad (4)$$

where  $\tau = 1/(\alpha + \beta)$ , the relaxation time constant,  $\omega = 2\pi f$ ,  $j$  is  $-1$  and  $f$  is frequency.

In general for multiple ionic conductances:

$$Y = j\omega C + 1/R + \sum_i G_i/(1 + j\omega\tau_i). \quad (5)$$

It should be noted that  $G_i$ , as defined by the numerator of the last term of equation 4, is dependent explicitly on membrane potential,  $V$ , and is equal to zero if either  $V = V_e$  or the rate constants are not voltage dependent, i.e.  $\alpha_V$  and  $\beta_V$  are zero. Under these latter conditions the membrane is a passive RC circuit and is described by just the first two terms of equation 5. The passive membrane time constant is defined as  $RC$  when  $G_i = 0$  and  $R$  is the membrane resistance. In the case of one ionic conductance, as in equation 4, the term  $R$  of equation 5 will include both the passive resistance and the voltage-dependent second term of equation 4, i.e. the steady-state conductance. Although chord conductances are always positive, the slope conductance at a particular value of the membrane potential can be positive, negative or zero. A negative value occurs when the driving force ( $V - V_e$ ) of the third term of equation 4 is negative.

The experimental results provide a basis for the estimation of membrane parameters that can be incorporated into Hodgkin-Huxley type equations (Traub, 1982; Traub and Wong, 1983) to be used for simulation studies. In our experiments two relaxation terms were required to fit the impedance measured in the presence of NMDA, one with a negative conductance (Fishman *et al.* 1983) and the other a slower positive conductance (see Fig. 4). Tentatively, we can identify the negative conductance term with sodium and calcium ions flowing through the NMDA channel complex and the positive conductance term as a voltage-activated potassium conductance, which is modeled here as one channel but clearly consists of at least a delayed rectifier and a calcium-activated potassium system. The results reported in this paper were fitted well with one positive and one negative conductance.

### Neuronal models

The experimental driving point function data were interpreted with a Rall-type lumped soma-equivalent cylinder model as a minimal representation of a neuron (Rall, 1959, 1969; Redman, 1973), i.e. a reduced neuron. These models provide a mathematical description of a neuron that can be used to predict the potential response to a synaptic input located at different electrotonic lengths from the soma. Furthermore, the data are measured at different membrane potentials and, therefore, model simulations can be used to predict the effect of voltage-dependent conductances on synaptic potential responses.

The experimental data were curve-fitted with a lumped soma-equivalent cylinder model consisting of eight equal compartments coupled to an isopotential cell body to obtain membrane parameters for both passive and active properties. Admittance functions described by equation 5, where  $i=1$  or  $2$ , were used for each compartment. In addition, there is a resistance,  $R_s$ , connecting each compartment. The number of parameters determined by the experimental data were as follows:  $C_m$  and  $T_c$ , the soma capacitance and ratio of compartmental to soma capacitance;  $R_m$  and  $T_r$ , the frequency-independent resistance of the soma and the ratio of compartmental to soma resistance;  $G_i$  and  $T_i$ , the amplitude of the frequency-dependent voltage-sensitive conductance of the soma and the ratio of the corresponding conductances in the compartments;  $\tau_i$ , the time constant for  $G_i$ , which was the same in both the soma and compartments; and finally,  $R_s$ . Unless otherwise stated,  $T_i=T_c$  and  $T_r=1/T_c$ . The electrotonic length ( $L$ ) was calculated from the square root of the ratio of the zero-frequency impedance of a dendritic compartment to  $R_s$  (see legend to Fig. 2 in Moore and Christensen, 1985). The computed  $L$  includes the steady-state values of the active conductances.

The curve-fitting procedures follow those previously published (Moore *et al.* 1988). The impedance of the compartmental representation of the cable was calculated by computing the impedance of the end segment, adding the series resistance connecting the segments, summing in parallel the impedance of the next compartment, and then repeating this procedure for each successive segment until finally the soma is reached (Moore and Christensen, 1985). Sensitivity analysis shows that chi square error functions have clear minima for all the parameters with the exception of the turning-off rate constant,  $\beta$ , of the potassium conductance (Murphey *et al.* 1992; see also Moore and Buchanan, 1993).

As discussed above, the relaxation times are equivalent to the usual voltage-clamp time constants that would be measured if a small signal isopotential step clamp were possible. Therefore, they represent activation or inactivation time constants of the specific ionic conductances defined by the rate constants of the underlying kinetic processes that determine the opening and closing of the various chemical and voltage-gated channels. This procedure was tested by correctly fitting analytically derived soma-equivalent cylinder data to show that both specific membrane and cable properties are obtained.

## Results

### *Dorsal cell*

#### *The impedance function near the resting membrane potential*

The dorsal cell is a primary sensory bipolar or unipolar neuron which, in the lamprey, is localized in the spinal cord (Freud, 1878; Rovainen, 1979). The dorsal cell could easily be identified as a large, approximately spherical cell near the midline. The results from the dorsal cell provide, in part, a control of the method since these cells have few or no processes and thus approach isopotential behavior. Fig. 2A shows the ratio of the input control voltage to the output current as sinusoidal voltage changes at different frequencies were applied during voltage clamp. This ratio is the impedance function and is composed of two parts, a magnitude and a phase difference between the sinusoidal voltage and

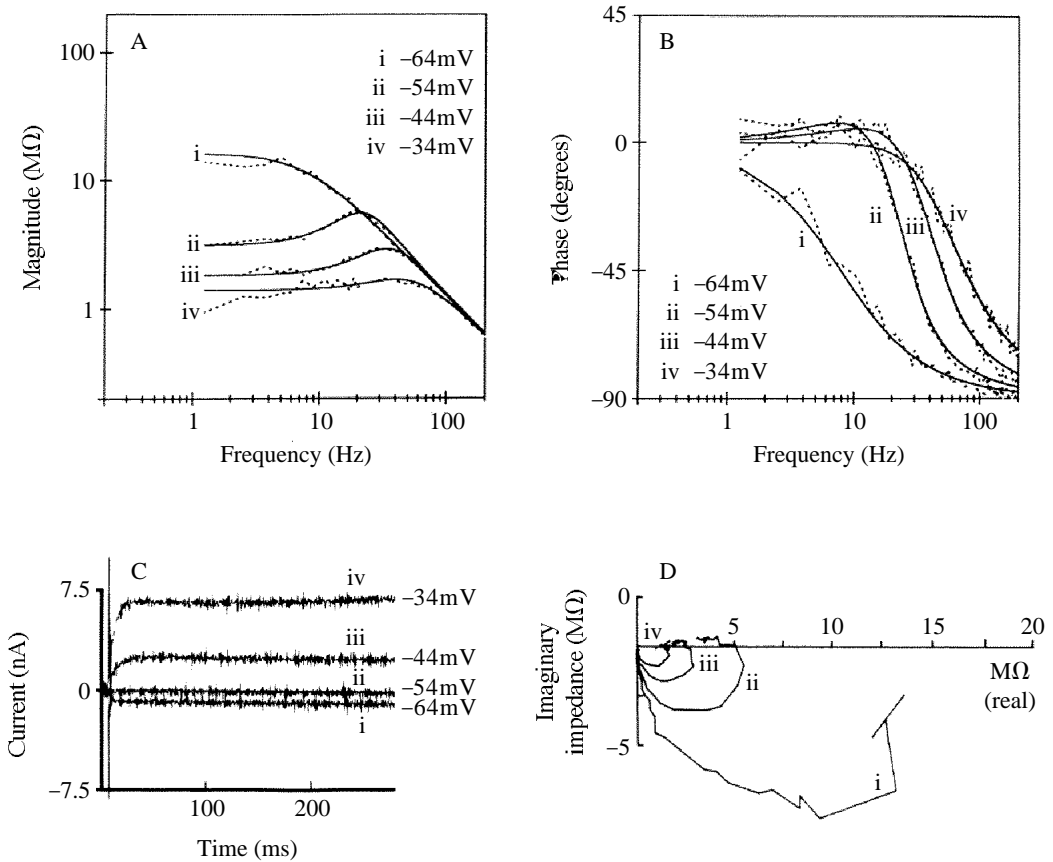


Fig. 2. Potential dependence of dorsal cell membrane properties. The voltage-clamp currents that occurred before the sum of sines stimulus was applied are illustrated in C. The outward current relaxation times are seen for the two depolarizations from the holding level ( $-54\text{mV}$ ) and correlate with the corresponding resonant peaks of the magnitude functions of A. A pronounced resonance was also seen at the holding level. The smooth curves through the data points of A and B are curve-fitted magnitude and phase functions for an isopotential single somatic compartment. The following parameters were used:  $C_m=3.2\text{nF}$  and  $R_m=17\text{M}\Omega$  at  $-64\text{mV}$ ;  $R_m=9.3\text{M}\Omega$ ,  $G_1=210\text{nS}$ ,  $\tau_1=31\text{ms}$  at  $-54\text{mV}$ ;  $R_m=4.3\text{M}\Omega$ ,  $G_1=320\text{nS}$ ,  $\tau_1=19\text{ms}$  at  $-44\text{mV}$ ;  $R_m=2.2\text{M}\Omega$ ,  $G_1=252\text{nS}$ ,  $\tau_1=12\text{ms}$  at  $-34\text{mV}$ . In addition to the magnitude and phase, an impedance plane plot is shown in D to illustrate two points: (1) the approach of data at high frequencies to the origin and (2) the semicircular shape of the plots. The former shows that the switching clamp effectively suppresses the electrode and the latter that the dorsal cell is essentially isopotential for the frequency band measured.

current, both of which vary with frequency. The amplitude of the dorsal cell response was relatively constant at low frequencies, but it gradually became smaller as the frequency increased. The phase relationship of the dorsal cell (Fig. 2B) was approximately in phase around 1Hz and showed a phase lag of nearly  $90^\circ$  at 100Hz.

The dominance of the soma in the dorsal cell (Fig. 2A,B) led to essentially isopotential, one-compartment behavior, like a simple RC circuit, at hyperpolarized values. The

passive RC behavior was indicated (Fig. 2A, trace i) by the magnitude of the impedance, which was flat at low frequencies and then fell off with frequency as a simple filter function with a corner frequency,  $f_c$  (defined as the frequency at half the low-frequency amplitude), proportional to the reciprocal of the membrane time constant,  $f_c=1/(2\pi RC)$ . The corresponding phase function went from 0 to  $-90^\circ$ , as is characteristic of a parallel RC circuit. Multiple compartments or cable circuits do not show this type of behavior (Jack *et al.* 1975).

The dorsal cell in Fig. 2 showed passive behavior if hyperpolarized to  $-64\text{mV}$ . In six of nine dorsal cells analyzed at their resting potential, passive behavior was observed. Although in the other three cells an RC circuit did not accurately describe the data at rest, passive behavior was observed if the cells were hyperpolarized by  $5\text{--}10\text{mV}$ , which may be closer to their normal resting level. In all cells tested, hyperpolarizations greater than  $10\text{mV}$  led to no additional changes in the impedance.

A one-compartment function consisting of only a parallel resistance and capacitance was fitted to the data of Fig. 2A,B, trace i. In the time domain, this function would give a single exponential voltage response to a current input with a time constant given by the product of the membrane resistance and capacitance. In contrast, the current response to a  $-10\text{mV}$  voltage-clamp step from the holding level of  $-54\text{mV}$  illustrated in Fig. 2C, trace iii, showed a constant current level. This finding supports the hypothesis that the voltage clamp of the dorsal cell provides an adequate isopotential control for the entire cell surface (space clamp). An inadequate space clamp would show some time-dependent behavior in the current response representing the charging of the uncontrolled potential in an unclamped cable.

### *Impedance functions at depolarized membrane potentials*

In Fig. 2A,B, the impedance functions were investigated at different levels of membrane potential from  $-64$  to  $-34\text{mV}$ . The magnitude of the impedance function decreased with depolarization as a consequence of an increased current response to a given voltage-clamp input. The low-frequency impedance decrease cannot be described as a simple conductance increase that alone could continue to show RC behavior, but instead showed an increased impedance at intermediate frequencies (resonance) well above the low-frequency values. Concomitant with the resonance in the magnitude function, the phase function (Fig. 2B, traces iii, iv) crossed zero at higher frequencies for more depolarized potentials.

The increased impedance at particular frequencies was the result of a decreased current response to an imposed voltage, i.e. an anti-resonance in the current was reflected as a resonance in the impedance ( $\delta V/\delta I$ ). This behavior was a direct consequence of a voltage-dependent kinetic process governing the activation of an outward current. This occurs when there is a minimum in the current as a function of the frequency of the voltage-clamped sinusoidal command. An explanation for such a resonance is that as the frequency increases the kinetics of the voltage-dependent gates do not allow them to be open long enough to pass current. As the frequency further increases, more current begins to flow in the capacitive element of the membrane. Thus, the anti-resonance of the

current is due both to the ionic conductance process being limited by frequency and to an increase in the passive capacitative current at high frequencies.

During a step depolarization, the dorsal cell shows the exponential development of an outward current with an activation time constant that decreases as the step potential becomes more positive. Magnitude and phase functions of the impedance show a clear shift of the resonance peak to higher frequencies with increasing depolarizations. Since the measurements were performed in the presence of TTX and during a net outward current, it is likely that the resonance is related to a potassium conductance. As pointed out above, in the frequency domain the addition of a voltage-dependent conductance to the passive resistance and capacitance leads to a resonating circuit.

The measured impedance functions of the dorsal cell at different levels of membrane potential (Fig. 2A,B) were fitted with an RC circuit plus the addition of a single voltage-dependent conductance (equation 4). The voltage-dependent relaxation time constants of the fitted functions ( $\tau$  of equation 4) decreased with membrane depolarization. The  $\tau$  values are comparable to the activation kinetics of the step voltage-clamp currents of Fig. 2C. At the hyperpolarized value of  $-64\text{mV}$  the data were fitted with an RC circuit alone, indicating that at potentials slightly hyperpolarized from rest the dorsal cell impedance is essentially passive.

#### *Space clamp shown with impedance plane plots*

The ability of a one-compartment model to fit the data is strong evidence that the switching voltage and single-electrode current-clamp provides an accurate measurement of the membrane properties of an intact neuron. Further evidence for the lack of electrode artifacts can be seen in an alternative representation of the data using complex arithmetic, namely the imaginary part *versus* the real part of the complex impedance (Fig. 2D). This graph is known as the impedance plane plot and is useful because both the asymptotes and the shape of the plot graphically reveal specific features of a measured circuit (Jack *et al.* 1975). In the dorsal cell measurements, the shape of the plot is that of a semicircle, indicating that the data are consistent with a single compartment. Frequency increases along the semicircle to the left towards the origin of the plot in Fig. 2D, in which i, ii, iii and iv represent the same data points as i–iv in Fig. 2A,B. If a single compartment were measured in series with a resistance, such as could occur with a microelectrode, the high-frequency intercept on the abscissa would have the value of the series resistance. In the measurements shown, the high-frequency asymptote approaches the origin, showing that there is no significant series resistance. Consequently, the switching system has been able effectively to remove the electrode impedance. These controls are important since electrode artifacts could easily be confused with dendritic cable structures attached to the soma (see Materials and methods for further details). In conclusion, the dorsal cell data serve as control measurements establishing the validity of the single-electrode switching method in determining the correct impedance function for neurons within an intact spinal cord.

#### *Neurons with branched dendrites*

The resting branched neuron shows a high-frequency (30–200Hz) phase function of

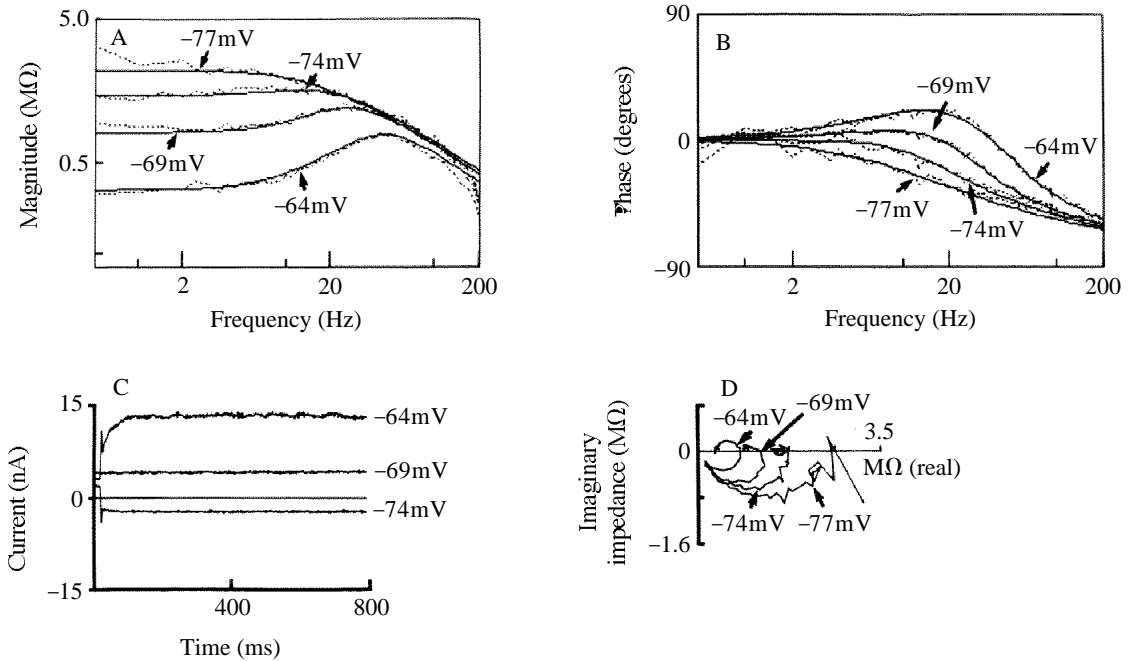


Fig. 3. Voltage-dependent neuron impedance functions under voltage-clamp conditions. (A,B) Four superimposed magnitude and phase functions from  $-77$  to  $-64$  mV with curve-fitted functions superimposed. The fitted functions had the following parameters:  $C_m=1.3$  nS,  $T_c=0.8$ ,  $R_m=9.8$  MΩ at  $-77$  mV;  $R_m=7.3$  MΩ,  $G_1=56$  nS,  $\tau_1=15$  ms at  $-74$  mV;  $R_m=4.5$  MΩ,  $G_1=292$  nS,  $\tau_1=14$  ms at  $-69$  mV;  $R_m=2.2$  MΩ,  $G_1=1520$  nS,  $\tau_1=16$  ms at  $-64$  mV. C shows step voltage-clamp currents from a branched neuron for a depolarizing step of 5 mV to  $-64$  mV and a hyperpolarizing step of 5 mV to  $-74$  mV. D illustrates the impedance plane plots for data from A and B. At  $-64$  mV the spiral loop shown in the upper right-hand quadrant (positive real and imaginary values) is a reflection of the resonance observed in A and B.

between  $30$  and  $90^\circ$  (Fig. 3B), characteristic of a cable structure attached to an isopotential cell body. Similarly, the impedance plane plot of Fig. 3D is a depressed semicircle that is a continuum between the semicircle of a dorsal cell and the  $45^\circ$  high-frequency limiting slope of an infinite cable. The impedance function of a branched neuron is best described as intermediate between that of an isopotential compartment and a cable, as would be expected from its composite structure. Thus, only a quantitative analysis of the shape of the impedance function with a particular model can reveal specific properties, which themselves will be variable as a result of the large number of different cell types within the spinal cord.

At the resting potential, most neurons did not show a resonance in the impedance function. Although no clear resonance was observed, rest appears not to be entirely a passive state. It can be seen from a comparison of the resting and hyperpolarized records of Fig. 3 that if the neuron is hyperpolarized the impedance tends to increase. Therefore, some ionic conductances must be active at rest and a fully passive state is only achieved

with hyperpolarization. Resonance will be present if the parameters of the voltage-dependent conductances are such that the impedance function is not critically damped.

Branched neurons did show a resonance at depolarizing potentials that elicited the activation kinetics of steady-state outward currents. Further depolarizations led to higher resonance frequencies, which is consistent with measurements previously reported on giant interneurons (Moore and Christensen, 1985). Fig. 3 shows potential-sensitive impedance functions that correlate well with the presence of an outward current that is activated with depolarization. The impedance data were analyzed with the reduced neuronal model to take into account the cable properties of the dendritic tree rather than erroneously to assume that the cell was space clamped. The curve fits for somatic depolarizations shown in Fig. 3 have a single positive voltage-dependent conductance that is uniformly distributed throughout the soma and cable. The fitted parameters gave a passive electrotonic length,  $L$ , for the hyperpolarized cell of 1.9 and outward current activation time constants of about 15ms. The curve fits for the depolarized neuron had electrotonic lengths of 2.7, 4.3 and 8.1 at  $-74$ ,  $-69$  and  $-64$ mV, respectively. Larger depolarizations were generally not examined under these conditions because the electrode could not pass sufficient current to hold the point voltage clamp. The finding that the values of  $L$  were significantly greater than 1 indicates that the membrane potential at the end of the equivalent cable is a fraction of its value in the soma. Therefore, the voltage-dependent, curve-fitted parameters are average approximations of the voltage-dependent parameters that are activated during a depolarization of the soma.

#### *Analysis of the effects of the excitatory amino acid agonist NMDA*

The inherent oscillatory nature of NMDA effects is markedly non-linear and generally requires the use of a voltage clamp to prevent oscillations (Moore *et al.* 1987a). The combination of a voltage clamp with the frequency domain (sum of sines) approach not only controls the potential and allows an estimate of the cable properties, but also reveals the natural tendency to oscillate shown by an enhancement of the impedance at a band of frequencies, namely a resonance, that occurs as a consequence of voltage-dependent conductances. Since the NMDA-induced conductances (both positive and negative) are steeply dependent on the membrane potential, it is evident that the holding level will greatly influence the voltage- or current-clamp response. In current-clamp measurements, it has been found that many neurons require a slight hyperpolarization before oscillations can be observed (Wallén and Grillner, 1987). This result is consistent with the observation that if the holding level was not hyperpolarized sufficiently, net inward currents were not observed with a step depolarization.

Fig. 4Ai–iii illustrates the effect of NMDA after a small hyperpolarization of  $-3$  mV on both the real time (Fig. 4Aiii) and frequency domain responses (Fig. 4Ai,ii). NMDA reduces the normal inward step current response, but, in this particular experiment, the inward current slowly increased to a steady-state value that was still less than that in the Ringer control (Fig. 4Aiii). The reduced current response is a reflection of the increased low-frequency impedance induced by NMDA.

In the presence of NMDA, the frequency domain measurements for the  $-3$  mV

hyperpolarization show an increased impedance and resonance (Fig. 4Ai,ii) as well as a clear indication of a negative conductance in the phase shift. The low-frequency phase function (Fig. 4Aii) is not only more negative than  $-90^\circ$  but even exceeds  $-180^\circ$ . By comparison, the control Ringer phase is near zero at low frequencies. The curve fits (smooth lines, Fig. 4Ai,ii) of the NMDA data required both a negative and a positive conductance with time constants of 6ms and 0.3s, respectively.

Fig. 4Bi,ii from another neuron illustrates that a hyperpolarization of  $-2$  mV compared to the holding level had a relatively small effect on the magnitude and phase functions. However, a  $+2$  mV depolarization (Fig. 4Ci,ii) showed clear evidence of a resonance response that was pronounced with a 4mV depolarization. The impedance magnitude was nearly 100-fold above that observed at a membrane potential 2mV more negative. The 0.5Hz resolution was just adequate to reveal this response, as shown in Fig. 4Ci by the greater than tenfold increase in impedance magnitude at the peak of the resonance compared to adjacent frequencies. Both inward and outward currents were increased in response to a 4mV potential step (Fig. 4Cii). The model fits shown for this neuron generally required both negative and positive conductances.

Although the neuron of Fig. 4B had no resonance at the holding potential or at  $-2$  mV, the phase functions were more than  $180^\circ$  negative at the lower frequencies. Thus, negative phase functions and the negative conductances associated with them do not always lead to a resonance, a condition that is critically determined by the interaction of inward and outward currents (Fishman *et al.* 1979). The resonant frequencies observed in the presence of NMDA at mean voltage-clamp potentials were within the frequency range of the spontaneous voltage oscillations (5–20mV) observed under current clamp. At larger depolarizations, the observed resonant frequencies of the impedance were progressively higher and tended to exceed those observed with spontaneous oscillations. As the membrane was progressively depolarized, the resonance was reflected in the phase function as an abrupt transition crossing  $0^\circ$  at the resonant peak frequency (Fig. 4Ci,ii).

Since the driving point function measurements probe the membrane with symmetrically small signals about any given membrane potential, it is possible to assess the state of the system at rest or at other steady-state potentials. In order to compare the transient responses to small voltage steps, the  $+2$  mV current was inverted and plotted in Fig. 4Biii with the  $-2$  mV record. In both cases there is a transient followed by a steady-state current essentially independent of the direction of the pulse. The symmetry of the current responses of the neuron in Fig. 4Biii to 2mV hyper- and depolarizations demonstrates that small membrane potential steps of the order of 1–2mV evoke linear responses that are required for the impedance analysis to be valid (Moore *et al.* 1980). The decreasing net outward current upon hyperpolarization also demonstrates that, at the holding level used, there were steady-state inward and outward currents that apparently did not inactivate and could be turned off or on by small potential steps. Thus, the net current in the presence of NMDA must be considered as the algebraic sum of currents in opposite directions. Further evidence of this behavior will be given below for currents measured in the absence of external sodium ions.

Small hyperpolarizations of  $-5$  mV or less did not turn off the NMDA-induced

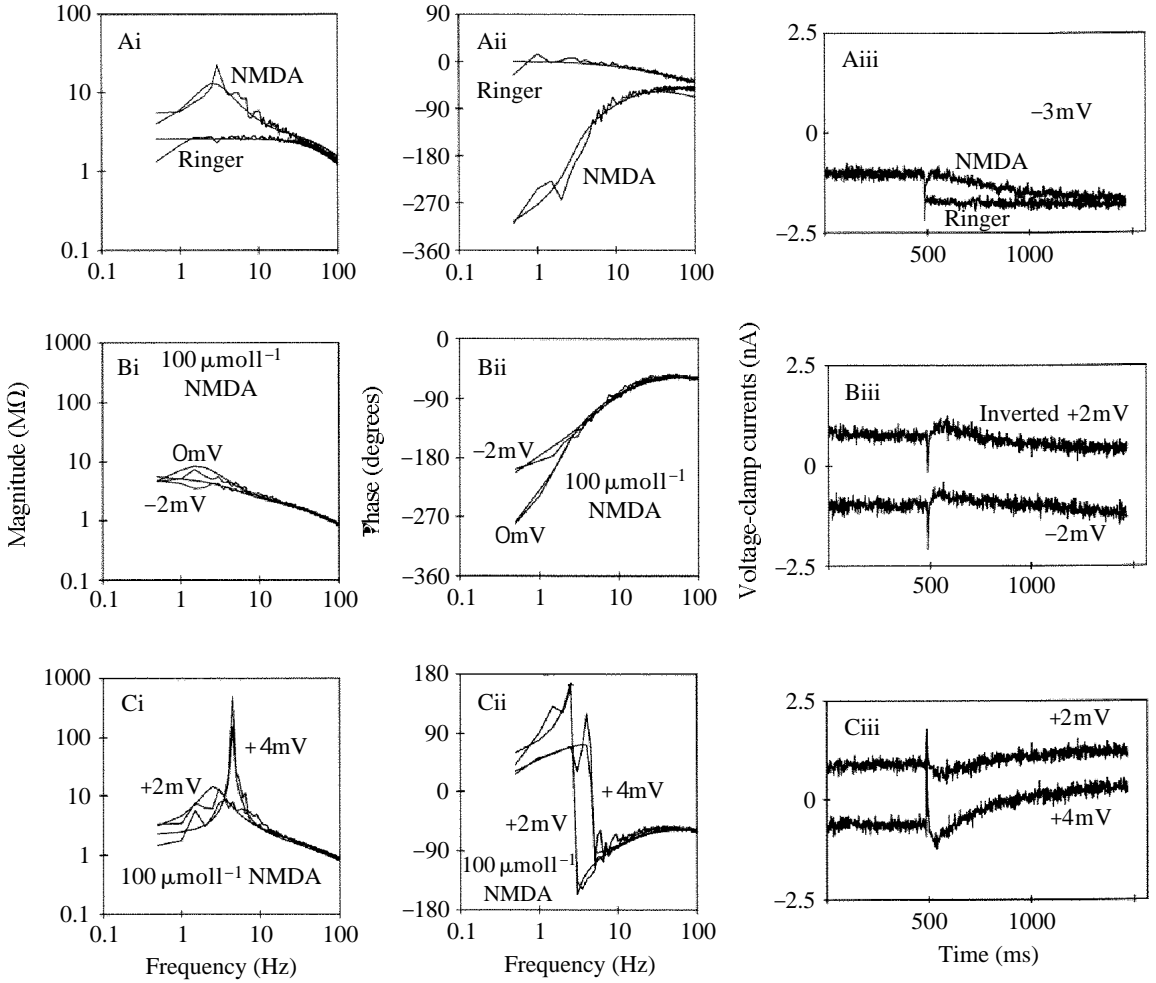


Fig. 4

negative conductance. However, a relatively large hyperpolarization of  $-13\text{mV}$  or greater was shown to be sufficient almost to abolish the negative conductance, as shown in the current records and phase plots in Fig. 5A. The superimposed voltage-clamp currents from a neuron were measured in the presence of  $100 \mu\text{mol l}^{-1}$  NMDA at two membrane potential steps,  $-5$  and  $-13\text{mV}$  (Fig. 5Aiii). Two superimposed hyperpolarizing currents are shown, indicating that  $-5\text{mV}$  relative to the holding level was insufficient to turn off the negative conductance, as can be seen from the essentially unchanged current level after the potential step. As in Fig. 4Aiii, Biii, there appears to have been a reduction of an inward current, suggesting that the  $-5\text{mV}$  step turned off part of the steady-state negative conductance. However,  $-13\text{mV}$  leads to a net inward current, relative to the holding current, consistent with a normal positive conductance. The corresponding phase functions of Fig. 5Aii are dramatically different. Net inward currents with depolarizing steps of  $2$ – $13\text{mV}$  were also observed (Fig. 5Biii, Ciii). The

Fig. 4. The effect of NMDA on the impedance function of a central neuron. Superimposed magnitude, phase and step-clamp currents for  $100 \mu\text{mol l}^{-1}$  NMDA and Ringer control solutions. NMDA induces a prominent resonance that manifests itself in the phase function as a sharp transition crossing zero. The potentials are given relative to the holding level, which was  $-50\text{mV}$  except in Ringer's solution at  $-60\text{mV}$ . (Ai) NMDA induces a marked increase in the impedance magnitude as a result of the activation of a negative conductance as indicated by the negative phase function shown in Aii. The smooth curve fits through the data have the following parameter values: in Ringer's solution at  $-3\text{mV}$ ,  $C_m=0.7\text{nF}$ ,  $R_m=3.1\text{M}\Omega$ ,  $R_s=2.6\text{M}\Omega$ ,  $T_c=1.9$  and  $T_r=2.5$ ; in NMDA,  $C_m=0.7\text{nF}$ ,  $R_m=5.5\text{M}\Omega$ ,  $G_1=-340\text{nS}$ ,  $T_1=6\text{ms}$ ,  $G_2=320\text{nS}$ ,  $T_2=0.3\text{s}$ ,  $R_s=4.4\text{M}\Omega$ ,  $T_c=1.9$  and  $T_r=0.3$ . (Aiii) The current response with NMDA shows a rapid transient followed by the slow development of a steady-state current. The hyperpolarization responses of Aiii show no transients in Ringer's solution in contrast to the slow development of a reduced inward current in NMDA. (Bi,ii) Superimposed magnitude and phase functions for holding and  $-2\text{mV}$  hyperpolarization. In B and C the voltage-independent curve-fitted parameters were:  $C_m=1.0\text{nF}$ ,  $R_s=1\text{M}\Omega$ ,  $T_c=1.7$  and  $T_r=0.6$ . The voltage-dependent curve-fitted parameters were as follows: at  $-2\text{mV}$ ,  $R_m=110\text{G}\Omega$ ,  $G_1=-96\text{nS}$ ,  $T_1=1.0\text{ms}$ ,  $G_2=35\text{nS}$ ,  $T_2=978\text{ms}$ ; at  $0\text{mV}$ ,  $R_m=7.5\text{G}\Omega$ ,  $G_1=-92\text{nS}$ ,  $T_1=1.4\text{ms}$ ,  $G_2=80\text{nS}$ ,  $T_2=551\text{ms}$ . (Biii) Voltage-clamp currents in response to  $\pm 2\text{mV}$  depolarizations. The  $+2\text{mV}$  response has been inverted and offset. (Ci,ii) Magnitude and phase functions for 2 and  $4\text{mV}$  depolarizations. The voltage-dependent curve-fitted parameters were as follows: at  $+2\text{mV}$ ,  $R_m=0.8\text{G}\Omega$ ,  $G_1=-88\text{nS}$ ,  $T_1=1\mu\text{s}$ ,  $G_2=136\text{nS}$ ,  $T_2=474\text{ms}$ ; at  $+4\text{mV}$ ,  $R_m=30\text{G}\Omega$ ,  $G_1=-76\text{nS}$ ,  $T_1=1\mu\text{s}$ ,  $G_2=204\text{nS}$ ,  $T_2=259\text{ms}$ . (Ciii) Voltage-clamp currents in response to 2 and  $4\text{mV}$ . The  $2\text{mV}$  response was offset from the baseline level given by the  $4\text{mV}$  response.

most hyperpolarized case was curve fitted with a completely passive model (Moore and Christensen, 1985) typified by a phase function near zero at low frequencies. In contrast, the  $-5\text{mV}$  phase function is nearly  $-180^\circ$  at lower frequencies and was fitted with active negative and positive conductances.

The dependence of the resonance upon potential in an NMDA-activated neuron is illustrated by Fig. 5Ai,Ci for changes relative to the holding level from  $-13$  to  $+13\text{mV}$ . The observed resonant frequencies ranged from about  $1\text{Hz}$  at  $+2\text{mV}$  (Fig. 5Bi) to nearly  $5\text{Hz}$  at  $+13\text{mV}$  (Fig. 5Ci). As the membrane potential proceeds from its most hyperpolarized values to increasing levels of depolarization, the neuron first shows a clear negative conductance revealed by the phase function at  $-5\text{mV}$  (Fig. 5Aii) and  $+2\text{mV}$  (Fig. 5Bii), then a sharp resonance and discontinuous phase function at  $+6\text{mV}$  and, finally, at  $+13\text{mV}$ , a broader resonance with a less abrupt phase change (Fig. 5Cii). Both the magnitude resonances and the phase functions that cross zero at  $+6$  and  $+13\text{mV}$  correspond to the oscillatory behavior of this cell seen under current-clamp conditions. At more positive potentials the peaks of the resonances occur at higher frequencies, consistent with the finding that, under current clamp, neurons that oscillate in TTX and NMDA do so at higher frequencies upon depolarization (Wallén and Grillner, 1987). The curve fits of these data required both positive and negative conductances with voltage-dependent time constants. The activation time constants of the negative conductance were in the millisecond to sub-millisecond range and the time constants for the outward conductance were in the range of seconds. In general, there was a 10–100-fold slower response for the positive conductance compared to the negative conductance, with the resonant frequency correlating to the slow conductance.

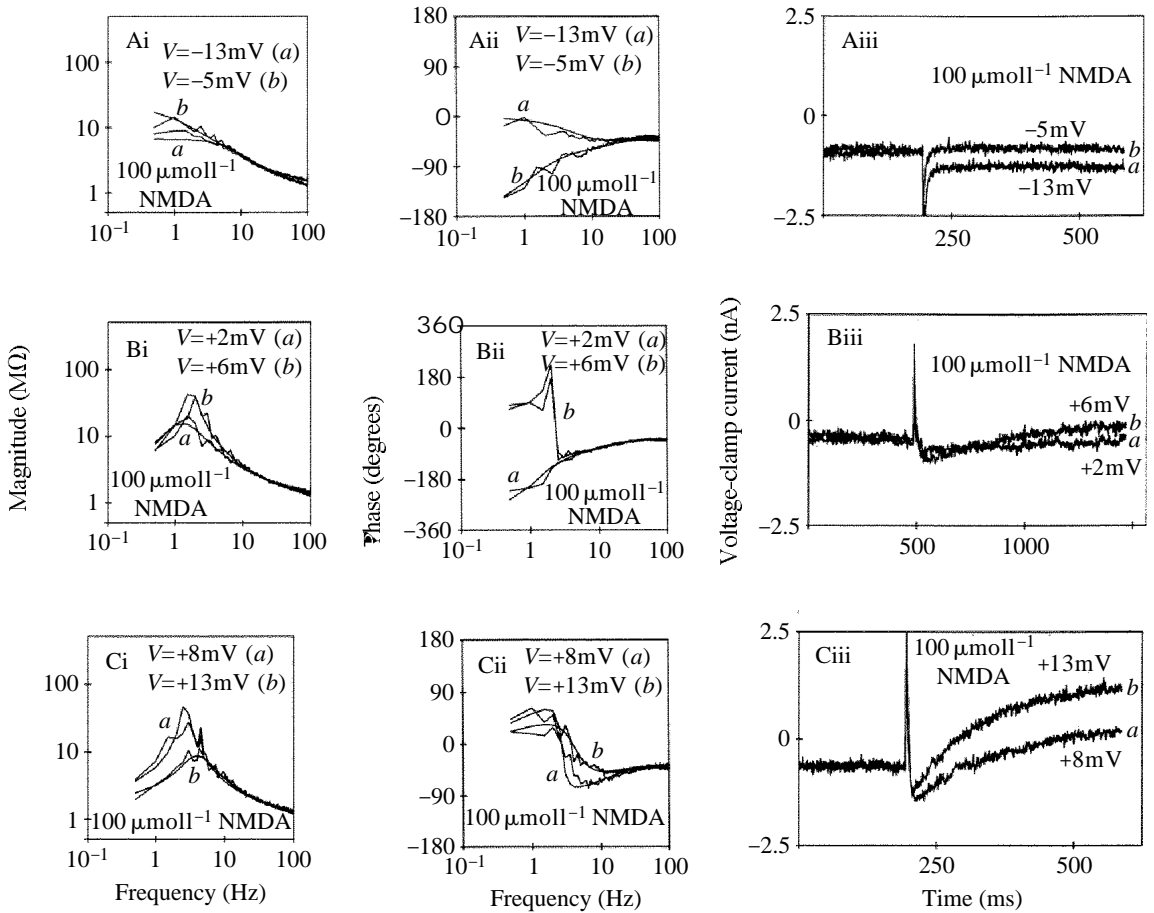


Fig. 5

### Effect of external sodium ions on NMDA responses

Sodium is required for oscillations in spinal neurons bathed in TTX and NMDA (Wallén and Grillner, 1987). The 10mV step depolarization shown in Fig. 6Aiii shows a small inward transient current that is presumably carried by both  $\text{Na}^+$  and  $\text{Ca}^{2+}$  and virtually no steady-state current. Voltage-clamp currents of Fig. 6Biii measured in the absence of external  $\text{Na}^+$  indicate a reduction in the NMDA-induced inward current that un masks the presence of an outward current. The difference between these two currents is plotted in Fig. 6D as the NMDA-induced  $\text{Na}^+$  current for a 10mV depolarization. In the presence of a normal sodium concentration, the NMDA-induced inward and outward currents are of comparable magnitude; therefore, the total current response in normal Ringer's solution with NMDA is relatively small. Larger depolarizations (not shown) of 15mV and 20mV also caused an increased outward current when external sodium ions were removed. The increase in the steady-state voltage-clamp currents when sodium ions were removed appears to be a direct consequence of a decrease in inward  $\text{Na}^+$  current.

Fig. 5. The effect of potential on the NMDA-induced negative conductance. The potentials are given relative to the holding level of  $-50\text{mV}$ . The voltage-clamp currents in response to  $-5\text{mV}$  are virtually unchanged in the steady state from the holding level. However, at  $-13\text{mV}$ , a clear inward current more negative than the holding level is observed. The magnitude functions for these two potentials show that at low frequencies the impedance at  $-5\text{mV}$  is greater than that at  $-13\text{mV}$  as a result of the effect of a hyperpolarization that turns off an active negative conductance. The increased magnitude at  $-5\text{mV}$  is a consequence of the algebraic sum of the negative conductance and residual positive conductances leading to a net smaller conductance or greater impedance. The associated phase functions show a low-frequency value at  $-5\text{mV}$  that is more negative than  $-90^\circ$ . This is also an indication of a negative conductance. The phase function for  $-13\text{mV}$  returns to zero at low frequency, as expected for a passive circuit. Bi-iii and Ci-iii show additional depolarizations leading to a pronounced resonance that is dependent on the membrane potential. Curve fits with a reduced neuronal model for data from this cell gave the following values for the passive and active parameters:  $C_m=0.3\text{nF}$ ,  $R_s=0.6\text{M}\Omega$ ,  $T_r=0.5$  and  $T_c=2.2$  for all potentials; Ai,ii at  $-13\text{mV}$ ,  $R_m=98\text{M}\Omega$ ; Bi,ii at  $-5\text{mV}$ ,  $R_m=186\text{M}\Omega$ ,  $G_1=-6.6\text{nS}$ ,  $T_1=27\text{ms}$ ,  $G_2=92\text{nS}$ ,  $T_2=640\text{s}$ ; at  $+2\text{mV}$ ,  $R_m=200\text{M}\Omega$ ,  $G_1=-8\text{nS}$ ,  $T_1=8.8\text{ms}$ ,  $G_2=580\text{nS}$ ,  $T_2=29\text{s}$ ; at  $+6\text{mV}$ ,  $R_m=75\text{M}\Omega$ ,  $G_1=-15\text{nS}$ ,  $T_1=2.4\text{ms}$ ,  $G_2=34\text{nS}$ ,  $T_2=1.0\text{s}$ ; Ci,ii at  $+8\text{mV}$ ,  $R_m=45\text{k}\Omega$ ,  $G_1=-22\text{nS}$ ,  $T_1=1.9\text{ms}$ ,  $G_2=38\text{nS}$ ,  $T_2=0.5\text{s}$ ; at  $+13\text{mV}$ ,  $R_m=42\text{k}\Omega$ ,  $G_1=-18\text{nS}$ ,  $T_1=2.4\text{ms}$ ,  $G_2=52\text{nS}$  and  $T_2=0.3\text{s}$ .

The hyperpolarizing ( $-10\text{mV}$ ) voltage-clamp current of Fig. 6Aiii shows an NMDA effect similar to that of Fig. 4, in which there is no inward current and possibly a slight outward current response. In the  $\text{Na}^+$ -free solution, Fig. 6Biii illustrates a clear inward current on hyperpolarization ( $-10\text{mV}$ ) that is associated with an impedance function in Fig. 6Bi and Bii whose phase function approaches zero at low frequencies. In contrast, the impedance function for a  $-10\text{mV}$  hyperpolarization in the presence of external sodium ions (Fig. 6Aii) has a phase that is indicative of a negative conductance, i.e. values greater than  $-90^\circ$  at low frequencies. The curve fits for the  $-10\text{mV}$  hyperpolarizations in normal- $\text{Na}^+$  solution required active positive and negative conductances, but the response in zero- $\text{Na}^+$  solution was fitted with only a positive conductance that was identical to that used in normal- $\text{Na}^+$  solution.

The impedance function of Fig. 6Ai for the  $10\text{mV}$  depolarization in normal- $\text{Na}^+$  solution shows a resonance. In zero- $\text{Na}^+$  solutions the resonance is still present and at a higher frequency (Fig. 6Bi), though not as pronounced, as can be seen from the more damped magnitude function of Fig. 6Bi and the lack of a sharp phase transition in Fig. 6Bii. These results suggest that the resonance produced by the balance between negative and positive conductances is more pronounced than that of a predominantly positive conductance system. Furthermore, the lower magnitude of the impedance function in zero external  $\text{Na}^+$  indicates a higher conductance consistent with the larger steady-state current. The curve fits for these two conditions had identical positive conductances, but the negative conductance term in low- $\text{Na}^+$  solution contributed less, as can be seen from the quantitative values given in the legend of Fig. 6. In the presence of sodium ions and NMDA, the resonance is a mixture of outward and inward current kinetics, the combination of which leads to a lower peak frequency (Fig. 6Ai) the greater the inward current.

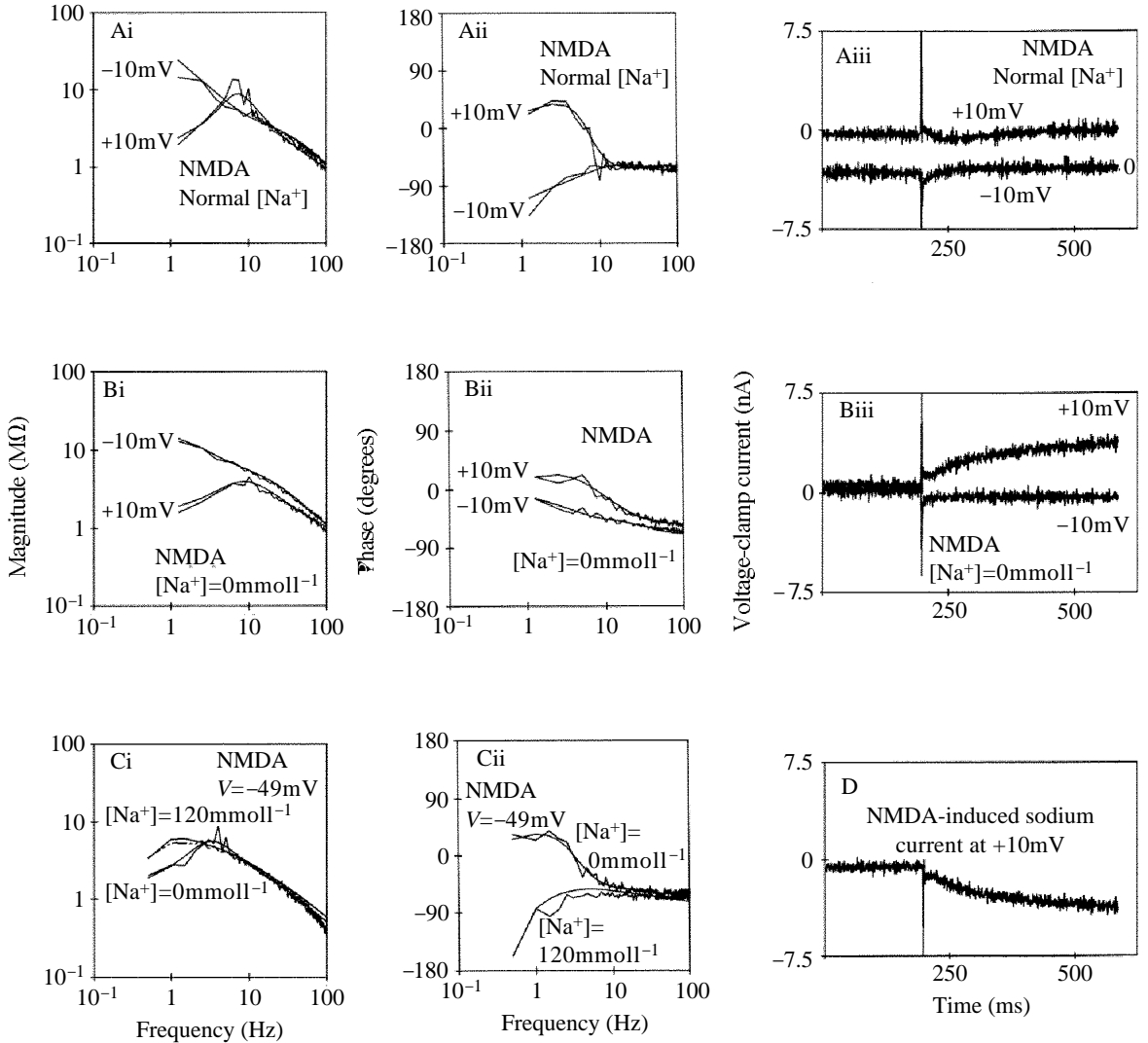


Fig. 6

In order to observe the effect of Na<sup>+</sup> removal on the impedance at the same absolute membrane potential, the superimposed magnitude and phase functions of Fig. 6Ci and Cii were measured at -49mV. In normal external Na<sup>+</sup>, a -5mV hyperpolarizing step was used from the resting level of -44mV, and in zero external Na<sup>+</sup>, the step was a +5mV depolarization from the resting level of -54mV. The difference in resting levels shows that an NMDA-activated Na<sup>+</sup> conductance contributes significantly to the depolarizing effect of NMDA activation. The curve fits of Fig. 6Ci and Cii illustrate that the removal of external sodium ions can be described by a reduction in the negative conductance induced by NMDA alone. This unmasking of the positive conductance led to a marked resonance of the magnitude function. Since these measurements were carried

Fig. 6. The role of sodium ions in the NMDA-dependent currents and impedances. The potentials are given relative to the holding levels of  $-44\text{mV}$  for normal-sodium and  $-54\text{mV}$  for low-sodium solutions. All solutions used in these experiments contained  $5\text{mmol l}^{-1}$  tetraethylammonium chloride ( $\text{TEA}^+$ ) in addition to the normal composition. In the low-sodium solutions the  $\text{NaCl}$  was replaced by  $111\text{mmol l}^{-1}$  Tris chloride. (Ai) Impedance magnitude responses for symmetrical voltage-clamp steps of  $\pm 10\text{mV}$  in  $100\ \mu\text{mol l}^{-1}$  NMDA and normal sodium ion concentration, showing a pronounced resonance for the depolarization. (Aii) Corresponding phase functions for  $\pm 10\text{mV}$  steps, indicating a negative phase function due to the negative conductance for the hyperpolarization response. (Aiii) Nearly symmetrical voltage-clamp currents for the  $\pm 10\text{mV}$  steps with almost no steady-state current, as would be expected for a high membrane impedance caused by a negative conductance. The  $-10\text{mV}$  trace has been offset with zero current level given at the right. (Bi) An impedance resonance for  $+10\text{mV}$  is illustrated, but the amplitude is smaller than that observed in Ai. (Bii) The removal of external sodium ions abolished the pronounced negative phase seen at low frequencies in Aii. (Biii) The zero sodium ion solution unmasked an outward current for the  $+10\text{mV}$  depolarization and led to a negative current for the  $-10\text{mV}$  hyperpolarization. (Ci) Comparison of impedance magnitudes in NMDA at the same absolute membrane potential of  $-49\text{mV}$  with and without external sodium ions. The removal of sodium ions reveals a more pronounced resonance not seen at this potential in normal Ringer's solution. (Cii) The phase functions for the magnitude of Ci show pronounced negative values in high- $\text{Na}^+$  solution. (D) The NMDA-induced sodium current calculated by subtracting the  $+10\text{mV}$  current in zero  $\text{Na}^+$  in Biii from the  $+10\text{mV}$  current in normal  $\text{Na}^+$  in Aiii. The reduced model curve fits for this data from an identified motoneuron had the following values:  $C_m=0.9\text{nS}$ ,  $R_s=1.4\text{M}\Omega$ ,  $T_c=0.7$  for the voltage-independent parameters; Ai and Aii at  $+10\text{mV}$ ,  $G_1=280\text{nS}$ ,  $T_1=95\text{ms}$ ,  $G_2=-330\text{nS}$ ,  $T_2=115\text{ms}$ ,  $R_m=3.2\text{M}\Omega$ ; Bi and Bii at  $+10\text{mV}$  with zero  $\text{Na}^+$ ,  $G_1=280\text{nS}$ ,  $T_1=95\text{ms}$ ,  $G_2=-210\text{nS}$ ,  $T_2=1.7\text{ms}$ ,  $R_m=3.6\text{M}\Omega$ ; Ai and Aii at  $-10\text{mV}$ ,  $G_1=17\text{nS}$ ,  $T_1=9\text{ms}$ ,  $G_2=-87\text{nS}$ ,  $T_2=1.1\text{ms}$ ,  $R_m=15\text{M}\Omega$ ; Bi and Bii at  $-10\text{mV}$  with zero  $\text{Na}^+$ ,  $G_1=17\text{nS}$ ,  $T_1=9\text{ms}$ ,  $G_2=0\text{nS}$ ,  $R_m=12\text{M}\Omega$ ; Ci and Cii for  $[\text{Na}^+]=120\text{mmol l}^{-1}$ ,  $G_1=489\text{nS}$ ,  $T_1=0.17\text{s}$ ,  $G_2=-470\text{nS}$ ,  $T_2=0.15\text{s}$ ,  $R_m>100\text{M}\Omega$ ; Ci and Cii for  $[\text{Na}^+]=0$ ,  $G_1=489\text{nS}$ ,  $T_1=0.17\text{s}$ ,  $G_2=-107\text{nS}$ ,  $T_2=0.14\text{s}$ ,  $R_m=25\text{M}\Omega$ .

out in the presence of  $\text{TEA}^+$ , the observed positive conductance seen in low external  $\text{Na}^+$  is probably a consequence of a calcium current through the NMDA receptor channels as well as a voltage-dependent calcium conductance leading to a calcium-activated potassium current. An additional factor in the low- $\text{Na}^+$  experiments is the possible increase in internal calcium ion concentration due to the lack of a sodium-calcium exchange pump, which could be important in maintaining low intracellular calcium levels.

#### *Effect of NMDA on membrane potential responses to constant currents*

As a comparison to the voltage-clamp case and in order to observe the voltage responses of neurons in TTX and NMDA, some cells were analyzed under current-clamp conditions. In oscillating neurons, the measurements were possible between oscillations, if the frequency was less than  $1\text{Hz}$ . Fig. 7 shows potential responses to step depolarizing currents for two cells bathed in NMDA; one that did oscillate (Fig. 7A) and another that did not (Fig. 7B). The potential response of the non-oscillating neuron was similar to that observed in normal Ringer's solution, showing a rather passive response to small

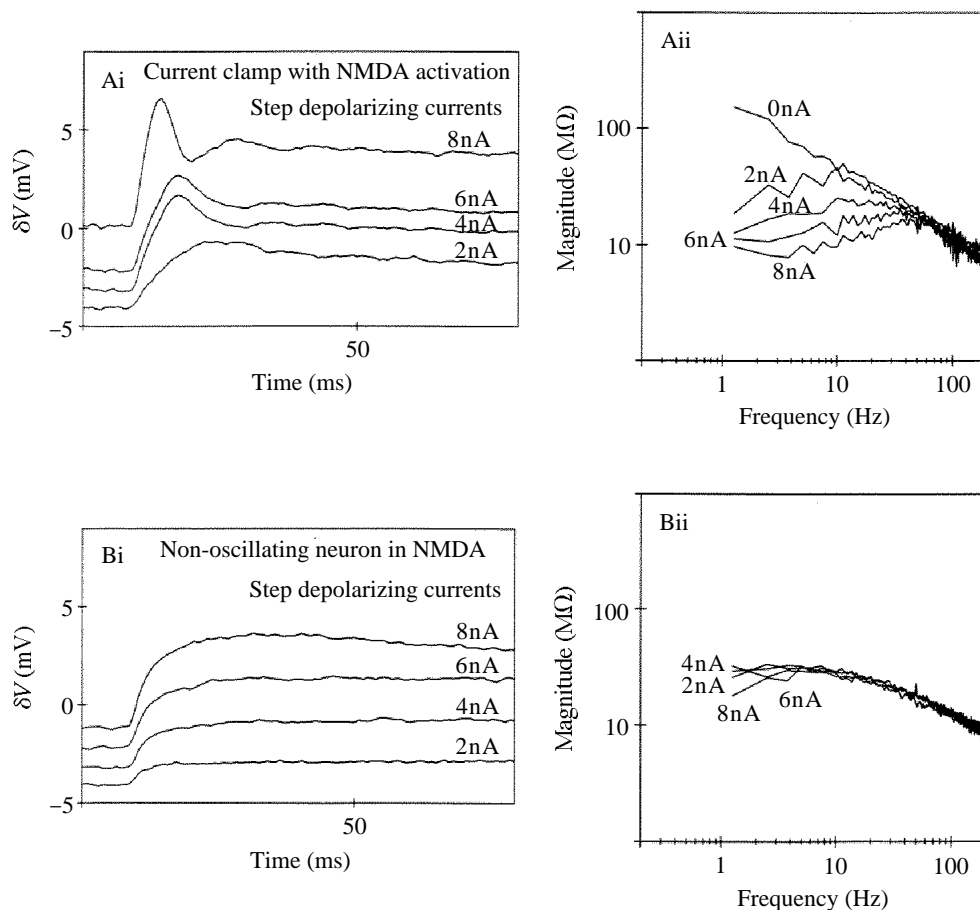


Fig. 7. Current-clamp responses during NMDA activation. (Ai) Measurements from a neuron bathed in  $100 \mu\text{mol l}^{-1}$  NMDA that showed spontaneous oscillations. Damped oscillatory responses are shown for the indicated step clamp currents. The potential between oscillations was  $-68\text{mV}$ . (Aii) Impedance functions for the same constant currents compared to the resting condition. The depolarizing currents lead to resonances that progressively increase in frequency as with the damped oscillations. (Bi) Measurements from another neuron in  $100 \mu\text{mol l}^{-1}$  NMDA that did not show any spontaneous oscillations or potential responses to the application of the agonist. The resting potential was  $-76\text{mV}$ . (Bii) Corresponding magnitude functions for Bi indicating minimal potential dependence. The results are comparable to those observed for all cells in normal Ringer's solution without NMDA.

depolarizing currents and a slight hint of a damped oscillation with large currents of  $8\text{nA}$  or greater (Fig. 7Bi). The magnitude functions for these step currents were relatively insensitive to voltage, showing a broad resonance for the largest depolarization in response to  $8\text{nA}$ . In contrast, the oscillating neuron of Fig. 7Ai showed damped oscillations in response to depolarizing currents and corresponding resonance impedance functions that were strongly potential-dependent.

The similarity of the impedance functions between oscillations during current clamp to those seen under voltage-clamp conditions (cf. Fig. 5Ai,Bi) indicates that uncontrolled

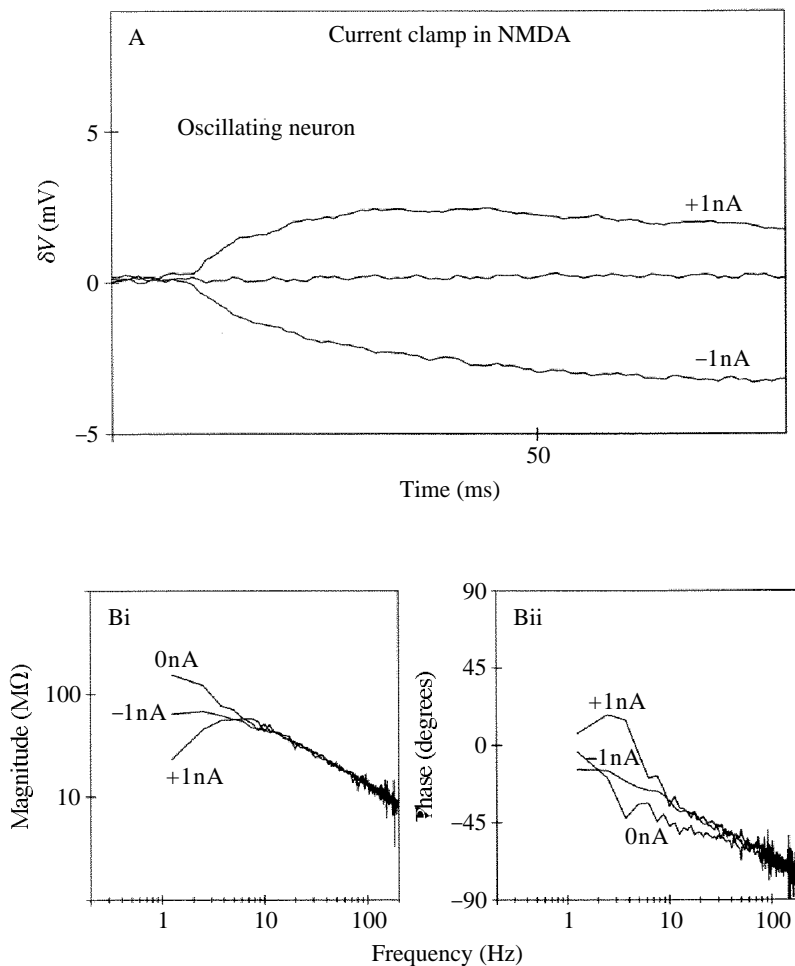


Fig. 8. Comparison of symmetrical constant-current responses during the activation of NMDA receptors. (A) Asymmetrical potential responses to  $\pm 1$ nA currents of the neuron of Fig. 7A illustrate the potential-dependent conductances. (Bi) The corresponding impedance magnitude functions show that the resting condition (0nA) has the highest magnitude. (Bii) The phase functions show that the most negative phase is associated with 0nA. The  $-1$  nA current decreases the negative conductance, but the  $+1$ nA current clearly activates voltage-dependent conductances with the net effect being a decrease in the magnitude of the conductance.

oscillations, possibly present in distal regions of the dendrites when the soma was voltage-clamped, did not significantly distort the impedance measurements. The NMDA-induced damped oscillation in the potential response to a constant depolarizing current stimulus (Fig. 7A) is in marked contrast to the overdamped response observed in normal Ringer's solution. This result is the current-clamp correlate to the resonance observed under voltage-clamp conditions.

Fig. 8A illustrates asymmetrical potential responses to  $\pm 1$ nA paired step currents of the oscillating neuron of Fig. 7A. The associated impedance functions of Fig. 8Bi,ii show

no resonance for the resting and hyperpolarized conditions, which is consistent with the non-oscillatory response to  $-1$  nA of Fig. 8A. Compared to the resting condition, the low-frequency impedance magnitude (Fig. 8Bi) decreased with a hyperpolarizing current of  $-1$  nA and the phase function (Fig. 7Bii) was less negative at low frequencies. These effects represent the turning off of a negative conductance with hyperpolarization. In contrast, the damped oscillatory response to  $+1$  nA of current (Fig. 8A) is reflected in the impedance as a resonance of the magnitude (Fig. 8Bi) and a zero crossing of the phase function (Fig. 8Bii). These results are in marked contrast to the much smaller potential sensitivity seen with non-oscillating neurons.

### Discussion

Frequency domain analysis provides a basis for understanding both the passive electrical properties imposed by the geometrical structure of neurons and the voltage-dependent ionic conductances determined by ion channel kinetics. The impedance measurements provide a means to assess the uniformity of the membrane potential of a neuron achieved during a point voltage clamp of the soma. Among the cells measured, only the dorsal cells can be considered isopotential. In these cells, step voltage-clamp currents could be analyzed over the frequency range 0–500Hz, limited primarily by the transients of the switching clamp (see Materials and methods) that are imposed by the properties of the electrodes and not the structure of the cell. Frequencies in the kilohertz range may require consideration of the bipolar axons of these cells. However, the electrodes used in these experiments precluded such high frequencies.

The analysis of the impedance data for branched neurons using a simple isopotential compartment with an eight-compartment single-cable structure gives an electrotonic length,  $L$ , of about 2 space constants. This is consistent with previous estimates of  $L$  for resting lamprey spinal cord neurons (Christensen and Teubl, 1979; Moore and Christensen, 1985). The data at different membrane potentials were accurately fitted with a homogeneous neuronal model. In Fig. 3 the model curve fits of the observed shift in resonance at different soma membrane potentials showed little change in the activation time constant. These results indicate that the model descriptions of the impedance functions represent an average of soma and dendritic kinetic parameters that accurately describe the experimental data. Furthermore, the curve fitting of the branched neurons required a cable structure in the model, showing that impedance measurements made with a single electrode in the soma reflected the dendritic structure.

The results presented here reflect the behavior of TTX-insensitive ionic processes that are dominated by potassium conductance systems. However, if there is sufficient activation of the sodium conductance or in the presence of agonists of neurotransmitters that activate other voltage-dependent conductances, the membrane properties will be significantly modified. Thus, neurons are capable of a significant change from a nearly passive condition at rest to the activation of ionic conductances that can lead to significant effects on their integrative behavior.

These conclusions emphasize the need for experimental measurements of membrane properties of intact whole cells in order to evaluate the basic mechanisms used in

processing synaptic inputs. It is not possible to know what aspects of channel properties are relevant to signal processing from isolated cell or patch measurements. The range of filter properties from tuning to phase reversals of negative conductances that can be predicted from known reasonable kinetic parameters is so widespread that it is likely that different types of neurons are uniquely specialized for their specific functions. Moreover, synaptic mechanisms can profoundly modify membrane properties such as that seen with the activation of NMDA receptors (Mayer and Westbrook, 1987*a,b*; Wallén and Grillner, 1987; Grillner *et al.* 1987*a,b*).

The NMDA-induced negative conductance is particularly apparent in the phase function, which approaches or passes  $180^\circ$  at low frequencies. This behavior is a function of a steady-state inward current in response to a depolarizing potential. That is, in contrast to a positive conductance, which would respond in phase, a negative conductance means that the response is opposite to that of a passive conductor and is therefore out of phase. One advantage of the frequency domain method is its sensitivity to a kinetic process such as a negative conductance. Many cells that did not show a net negative current response to a depolarizing step voltage clamp in the presence of NMDA had a phase function that indicated an active negative resistance. In addition to the phase reversal in NMDA, the observed impedance resonance also had a potential dependence analogous to that of the spontaneous voltage oscillations. Although resonance is a linear response and cannot be directly related to the non-linear voltage oscillations, the impedance function itself is a piece-wise linearization encompassing the potentials of NMDA-induced oscillations. The driving point function measurements show that, in the presence of NMDA, the resonance peak shifts from about 1 to 5Hz for a range of potentials 10–15mV about threshold. This is precisely the range of NMDA-induced oscillations seen in TTX and during fictive locomotion.

The analysis of NMDA experiments using a soma plus equivalent cylinder model with uniform voltage-dependent conductances was sufficient to describe a range of complicated driving point function behaviors. Most model fits of the impedance functions of neurons in NMDA gave a negative conductance with relaxation times in the millisecond or sub-millisecond range. In addition, the curve fits required a positive conductance whose relaxation time was of the order of hundreds of milliseconds or seconds. The slower relaxation process probably represents the development of an outward current that is in part dependent on NMDA activation. The rapid time constant for the NMDA-induced conductance is consistent with the expected kinetics of the NMDA-induced channel (Ascher and Nowak, 1988).

The finding that in NMDA a negative conductance remained with moderate hyperpolarizations (Fig. 4A) is consistent with the observation that oscillations were generally present in neurons for a limited potential range, often at a slight hyperpolarization from an NMDA-induced depolarization. It is the negative conductance and consequential inward current that must be present to induce an instability in the membrane potential so that it will depolarize and undergo spontaneous oscillations. If the membrane potential is such that there is insufficient net negative conductance then the neuron will not oscillate. The kinetics of the current response to a hyperpolarization are clearly complicated by the twofold effect of (1) increasing the magnesium block of the

NMDA channel with a probable decrease in the inward current, and (2) the decrease in the calcium-activated potassium current. If the NMDA-induced inward and outward currents can be reduced unequally by a hyperpolarizing step pulse, then the kinetics of the response could be due either to a magnesium block or to the removal of internal calcium ions, both of which would lead to an increase in an inward current with time as seen in Fig. 4Aiii and 4Biii. This effect is similar to the NMDA-induced tail currents that decrease with time after the end of a depolarizing pulse (Moore *et al.* 1987*a,b*; Hill *et al.* 1989). In normal Ringer's solution the potassium conductance is likely to be composed of at least two systems, the delayed rectifier and a calcium-activated conductance (Hill *et al.* 1985). In the presence of NMDA, an additional calcium current enhances the latter and, in combination with the negative conductances, leads to a highly oscillatory system.

The presence of a negative slope conductance results in a dynamic filtering process. A steady-state negative slope conductance typically exists in neurons owing to non-inactivating sodium and calcium ionic conductances. Since the conductances are in parallel, they are algebraically additive. Therefore, the net effect of an activation of a negative conductance is generally to reduce the total absolute slope conductance and in some instances even to reach a zero or net negative slope conductance. Using the reduced neuron model, the d.c. electrotonic length in the presence of NMDA becomes extremely short ( $<0.5$ ) or undefined if the d.c. impedance is less than zero. Whatever model might be used to compute an electrotonic length, if there are NMDA sites on the dendrites then the d.c. electrotonic length of the cell is likely to be much shorter in the presence of NMDA than in normal Ringer's solution. Thus, under normal physiological conditions the principal effect of a negative conductance would be to increase the membrane impedance so that the low-frequency synaptic potentials will become better propagated through the dendritic cable.

In conclusion, these experiments have shown that both the inherent and transmitter-induced voltage-dependent impedances markedly affect the cable properties of the neurons and therefore their ability to propagate synaptic potentials. In particular, activation of the NMDA receptor leads to an unstable condition where a negative conductance depolarizes the cell; this then turns on a repolarizing positive potassium conductance. The activation of both the NMDA-induced inward current and the potassium conductance contributes to a resonance in the impedance that will influence the inherent oscillation frequency. Finally, these experiments represent a first step in a quantitative analysis of the biophysical properties of individual neurons of the lamprey spinal cord.

This work was supported in part by the following grants DHHS-RO1MH45796, DHEW-NIH-2P01-NS-11255, NSF-BNS 83-16704, NSF INT-8513152 and an NIH Fogarty Senior International Fellowship Award to L.E.M.

### References

- ASCHER, P. AND NOWAK, L. (1988). The role of divalent cations in *N*-methyl-D-aspartate responses of mouse central neurons in culture. *J. Physiol., Lond.* **398**, 247–266.

- AULT, B., EVANS, R. H., FRANCIS, A. A., OAKES, D. J. AND WATKINS, J. C. (1980). Selective depression of excitatory amino acid induced depolarizations by magnesium ions in isolated spinal cord preparations. *J. Physiol., Lond.* **307**, 413–428.
- BEKKERS, J. M. AND STEVENS, C. F. (1989). NMDA and non-NMDA receptors are co-localized at excitatory synapses in cultured rat hippocampus. *Nature* **341**, 230–233.
- BRODIN, L. AND GRILLNER, S. (1985). The role of putative excitatory amino acid neurotransmitters in the initiation of locomotion in the lamprey spinal cord. I. The effects of excitatory amino acid antagonists. *Brain Res.* **360**, 139–148.
- BRODIN, L. AND GRILLNER, S. (1986). Effects of magnesium on fictive locomotion induced by activation of *N*-methyl-D-aspartate (NMDA) receptors in the lamprey spinal cord *in vitro*. *Brain Res.* **380**, 244–252.
- BRODIN, L., GRILLNER, S. AND ROVAINEN, C. M. (1985). *N*-Methyl-D-aspartate (NMDA), kainate and quisqualate receptors and the generation of fictive locomotion in the lamprey spinal cord. *Brain Res.* **325**, 302–306.
- BUCHANAN, J. T., BRODIN, L., DALE, N. AND GRILLNER, S. (1987). Reticulospinal neurones activate excitatory amino acid receptors. *Brain Res.* **408**, 321–325.
- BUCHANAN, J. T. AND COHEN, A. H. (1982). Activities of identified interneurons, motoneurons and muscle fibers during fictive locomotion in the lamprey and effects of reticulospinal and dorsal cell stimulation. *J. Neurophysiol.* **47**, 948–960.
- BUCHANAN, J. T. AND GRILLNER, S. (1987). Newly identified glutamate interneurons and their role in locomotion in the lamprey spinal cord. *Science* **236**, 312–314.
- CHRISTENSEN, B. N. AND TEUBL, W. P. (1979). Localization of synaptic input on dendrites of a lamprey spinal cord neurone from physiological measurements of membrane properties. *J. Physiol., Lond.* **297**, 319–333.
- CULL-CANDY, S. G. AND USOWICZ, M. M. (1987). Multiple-conductance channels activated by excitatory amino acids in cerebellar neurons. *Nature* **325**, 525–528.
- CULL-CANDY, S. G. AND USOWICZ, M. M. (1989a). Whole-cell current noise produced by excitatory and inhibitory amino acids in large cerebellar neurones of the rat. *J. Physiol., Lond.* **415**, 533–553.
- CULL-CANDY, S. G. AND USOWICZ, M. M. (1989b). On the multiple-conductance single channels activated by excitatory amino acids in large cerebellar neurones of the rat. *J. Physiol., Lond.* **415**, 555–582.
- DALE, N. (1986). Excitatory synaptic drive for swimming mediated by amino acid receptors in the lamprey. *J. Neurosci.* **6**, 2662–2675.
- DALE, N. AND GRILLNER, S. (1986). Dual component synaptic potentials in the lamprey mediated by excitatory amino acid receptors. *J. Neurosci.* **6**, 2653–2661.
- DALE, N. AND ROBERTS, A. (1984). Excitatory amino acid receptors in *Xenopus* embryo spinal cord and their role in the activation of swimming. *J. Physiol., Lond.* **348**, 527–543.
- DALE, N. AND ROBERTS, A. (1985). Dual-component amino acid-mediated synaptic potentials. Excitatory drive for swimming in *Xenopus* embryos. *J. Physiol., Lond.* **363**, 35–59.
- DINGLELINE, R. (1986). NMDA receptors: What do they do? *Trends Neurosci.* **9**, 47–49.
- FISHMAN, H. M., LEUCHTAG, H. R. AND MOORE, L. E. (1983). Fluctuation and linear analysis of Na current kinetics in squid axon. *Biophys. J.* **43**, 293–308.
- FISHMAN, H. M., POUSSART, D. AND MOORE, L. E. (1979). Complex admittance of Na<sup>+</sup> conduction in squid axon. *J. Membr. Biol.* **50**, 43–63.
- FISHMAN, H. M., POUSSART, D. J. M., MOORE, L. E. AND SIEBENGA, E. (1977). K<sup>+</sup> conduction description from the low frequency impedance and admittance of squid axon. *J. Membr. Biol.* **32**, 255–290.
- FLATMAN, J. A., SCHWINDT, P. C. AND CRILL, W. E. (1986). The induction and modification of voltage-sensitive responses in cat neocortical neurons by *N*-methyl-D-aspartate. *Brain Res.* **363**, 62–77.
- FOX, S. E. AND CHAN, C. Y. (1985). Location of membrane conductance changes by analysis of the input impedance of neurons. II. Implementation. *J. Neurophysiol.* **54**, 1594–1606.
- FREUD, S. (1878). Über Spinalganglien und Rückenmark des Petromyzon. *Sitzungsber Akad. Wiss. Wien* **78**, 81–167.
- GRILLNER, S., BRODIN, L., BUCHANAN, J. T., WALLÉN, P., DALE, N., HILL, R. AND MOORE, L. E. (1987a). Excitatory amino acid neurotransmission in the lamprey spinal cord a key role in the generation of locomotion. In *Excitatory Amino Acid Transmitters* (ed. P. Hicks, D. Lodge and H. McLennan), pp. 293–300. New York: Alan Liss, Inc.
- GRILLNER, S., MCCLELLAN, A., SIGVARDT, K., WALLÉN, P. AND WILÉN, M. (1981). Activation of NMDA-

- receptors elicits 'fictive locomotion' in lamprey spinal cord *in vitro*. *Acta physiol. scand.* **113**, 549–551.
- GRILLNER, S., MCCLELLAN, A., SIGVARDT, K., WALLÉN, P. AND WILLIAMS, T. (1982). On the neural generation of 'fictive locomotion' in a lower vertebrate nervous system, *in vitro*. In *Brain Stem Control of Spinal Mechanisms* (ed. B. Sjölund and A. Bökörklund), Fernström Foundation series, no. 1, pp. 273–295. New York, Oxford: Elsevier Biomedical Press.
- GRILLNER, S. AND WALLÉN, P. (1985). The ionic mechanisms underlying NMDA receptor induced, TTX resistant, membrane potential oscillations in lamprey neurones active during locomotion. *Neurosci. Lett.* **60**, 289–294.
- GRILLNER, S., WALLÉN, P., DALE, N., BRODIN, L., BUCHANAN, L. AND HILL, R. (1987*b*). Transmitters, membrane properties and network circuitry in the control of locomotion in lamprey. *Trends Neurosci.* **10**, 34–41.
- HILL, R. H., ÉRHEM, P. AND GRILLNER, S. (1985). Ionic mechanisms of three types of functionally different neurons in the lamprey spinal cord. *Brain Res.* **358**, 40–52.
- HILL, R. H., BRODIN, L. AND GRILLNER, S. (1989). Activation of *N*-methyl-D-aspartate (NMDA) receptors augments repolarizing responses in lamprey spinal neurons. *Brain Res.* **499**, 388–392.
- HODGKIN, A. L. AND HUXLEY, A. (1952). A quantitative description of membrane current and its application to conduction and excitation in nerve. *J. Physiol., Lond.* **117**, 500–544.
- JACK, J. J. B., NOBLE, D. AND TSJEN, R. W. (1975). *Electric Current Flow in Excitable Cells*. Oxford: Clarendon Press.
- JAHR, C. E. AND STEVENS, C. F. (1987). Glutamate activated multiple single channel conductance in hippocampal neurons. *Nature* **325**, 522–525.
- KOCH, C. (1984). Cable theory in neurons with active, linearized membranes. *Biol. Cybernetics* **50**, 15–33.
- LLANO, I., MARTY, A., JOHNSON, J. W., ASCHER, P. AND GÄHWILER, B. H. (1988). Patch-clamp recording of amino acid-activated responses in 'organotypic slice' cultures. *Proc. natn. Acad. Sci. U.S.A.* **85**, 3221–3225.
- LLINÁS, R. (1988). The intrinsic electrophysiological properties of mammalian neurons: insights into central nervous system function. *Science* **242**, 1654–1664.
- MACDERMOTT, A., MAYER, M., WESTBROOK, G., SMITH, S. AND BARKER, J. (1986). NMDA-receptor activation increases cytoplasmic calcium concentration in cultured spinal cord neurones. *Nature* **321**, 519–522.
- MACDONALD, J. F., PORIETIS, A. V. AND WOJTOWICZ, J. M. (1982). L-Aspartic acid induced a region of negative slope conductance in current–voltage relationship of cultured spinal cord neurons. *Brain Res.* **237**, 248–2532.
- MARMARELIS, P. Z. AND MARMARELIS, V. Z. (1978). *Analysis of Physiological Systems. The White Noise Approach*. New York: Plenum.
- MAURO, A., CONTI, F., DODGE, F. AND SCHOR, R. (1970). Subthreshold behavior and phenomenological impedance of the squid giant axon. *J. gen. Physiol.* **55**, 497–523.
- MAYER, M. L. AND WESTBROOK, G. L. (1985). The action of *N*-methyl-D-aspartic acid on mouse spinal neurones in culture. *J. Physiol., Lond.* **361**, 65–90.
- MAYER, M. L. AND WESTBROOK, G. L. (1987*a*). Permeation and block of *N*-methyl-D-aspartic acid receptor channels by divalent cations in mouse cultured central neurons. *J. Physiol., Lond.* **394**, 501–527.
- MAYER, M. L. AND WESTBROOK, G. L. (1987*b*). The physiology of excitatory amino acids in the vertebrate central nervous system. *Prog. Neurobiol.* **28**, 197–276.
- MOORE, L. E. AND BUCHANAN, J. T. (1993). The effects of neurotransmitters on the integrative properties of spinal neurons in the lamprey. *J. exp. Biol.* **175**, 89–114.
- MOORE, L. E. AND CHRISTENSEN, B. G. (1985). White noise analysis of cable properties of neuroblastoma cells and lamprey central neurons. *J. Neurophysiol.* **53**, 636–651.
- MOORE, L. E., FISHMAN, H. M. AND POUSSART, D. J. M. (1980). Small-signal analysis of K<sup>+</sup> conduction in squid axons. *J. Membr. Biol.* **54**, 157–164.
- MOORE, L. E., HILL, R. H. AND GRILLNER, S. (1986). Voltage-clamp analysis of NMDA induced oscillating spinal neurons. *Acta physiol. scand.* **128**, 20a.
- MOORE, L. E., HILL, R. H. AND GRILLNER, S. (1987*a*). Voltage clamp analysis of lamprey neurons – role of *N*-methyl-D-aspartate receptors in fictive locomotion. *Brain Res.* **419**, 397–402.

- MOORE, L. E., HILL, R. H. AND GRILLNER, S. (1987b). Voltage clamp frequency domain analysis of NMDA activated spinal neurons. *Soc. Neurosci. Abstr.* **428**, 12.
- MOORE, L. E. AND TSAI, T. D. (1983). Ion conductances of the surface and transverse tubular membranes of skeletal muscle. *J. Membr. Biol.* **73**, 217–226.
- MOORE, L. E., YOSHII, K. AND CHRISTENSEN, B. (1988). Transfer impedances between different regions of branched excitable cells. *J. Neurophysiol.* **59**, 689–705.
- MURPHEY, C. R., MOORE, L. E. AND BUCHANAN, J. T. (1992). A model of a lamprey neuron: parameter estimation on impedance data. *Soc. Neurosci. Abstr.* **539**, 3.
- NOWAK, L., BREGETOVSKI, P., ASCHER, P., HERBET, A. AND PROCHIANTZ, A. (1984). Magnesium gates glutamate activated channels in mouse central neurones. *Nature* **307**, 462–465.
- POUSSART, D., MOORE, L. E. AND FISHMAN, H. (1977). Ion movements and kinetics in squid axon. I. Complex admittance. *Ann. N.Y. Acad. Sci.* **303**, 355–379.
- RALL, W. (1959). Branching dendritic trees and motoneuron membrane resistivity. *Exp. Neurol.* **1**, 491–527.
- RALL, W. (1969). Time constants and electrotonic length of membrane cylinders and neurons. *Biophys. J.* **9**, 1483–1508.
- REDMAN, S. J. (1973). The attenuation of passively propagating dendritic potentials in a motoneurone cable model. *J. Physiol., Lond.* **234**, 637–664.
- ROVAINEN, C. M. (1974). Synaptic interactions of identified nerve cells in the spinal cord of the sea lamprey. *J. comp. Neurol.* **154**, 189–206.
- ROVAINEN, C. M. (1978). Mueller cells, 'Mauthner' cells and other identified reticulospinal neurons in the lamprey. In *Neurobiology of the Mauthner Cell* (ed. D. Faber and H. Korn), pp. 245–269. New York: Raven Press.
- ROVAINEN, C. M. (1979). Neurobiology of lampreys. *Physiol. Rev.* **59**, 1007–1077.
- SIGVARDT, K. A., GRILLNER, S., WALLÉN, P. AND VAN DONGEN, P. A. M. (1985). Activation of NMDA receptor elicits fictive locomotion and bistable membrane properties in the lamprey spinal cord. *Brain Res.* **336**, 390–395.
- TRAUB, R. D. (1982). Simulation of intrinsic bursting in CA3 hippocampal neurons. *Neuroscience* **7**, 1233–1242.
- TRAUB, R. D. AND WONG, R. K. S. (1983). Synchronized burst discharge in disinhibited hippocampal slice. II. Model of cellular mechanism. *J. Neurophysiol.* **49**, 459–471.
- WALLÉN, P. AND GRILLNER, S. (1987). N-Methyl-D-aspartate receptor-induced, inherent oscillatory activity in neurons active during fictive locomotion in the lamprey. *J. Neurosci.* **7**, 2745–2755.
- WALLÉN, P. AND WILLIAMS, T. L. (1984). Fictive locomotion in the lamprey spinal cord *in vitro* compared with swimming in the intact and spinal animal. *J. Physiol., Lond.* **347**, 225–239.
- WATKINS, J. C. (1981). Pharmacology of excitatory amino acid transmitters. In *Amino Acid Neurotransmitters* (ed. F. V. DeFeudis and P. Mandel), pp. 205–212. New York: Raven Press.
- WATKINS, J. C., EVANS, R. H., MEWETH, K. N., OLVERMAN, H. J. AND POOK, P. C. (1986). Recent advances in the pharmacology of excitatory amino acids. In *Excitatory Amino Acid Transmitters* (ed. P. Hicks, D. Lodge and H. McLennan), pp. 19–26. New York: Alan Liss, Inc.
- YOSHII, K., MOORE, L. E. AND CHRISTENSEN, B. (1988). Effect of subthreshold voltage-dependent conductances on the transfer function of branched excitable cells and the conduction of synaptic potentials. *J. Neurophysiol.* **59**, 706–716.